Properties of electrorheological suspensions based on conductive polymers.

Miroslav Mrlík

Master Thesis
2008

Tomas Bata University in Zlín
Faculty of Technology

Motto: Everything should be made as simple as possible, but not simpler.

Albert Einstein

I agree that the results of my master thesis should be used in the way my supervisor and the head of the department consider appropriate. Should the results be published, I would be included in the list of authors. I declare that I have completed this master thesis on my own and all used references have been cited.

In Zlín Signature

Univerzita Tomáše Bati ve Zlíně
Fakulta technologická
Ústav inženýrství polymerů
akademický rok: 2008/2009

ZADÁNÍ DIPLOMOVÉ PRÁCE
(PROJEKTU, UMĚLECKÉHO DÍLA, UMĚLECKÉHO VÝKONU)

Jméno a příjmení:	**Bc. Miroslav MRLÍK**
Studijní program:	**N 2808 Chemie a technologie materiálů**
Studijní obor:	**Inženýrství polymerů**
Téma práce:	**Vlastnosti elektroreologických suspenzí na bázi vodivých polymerů**

Zásady pro vypracování:

1. Provedení literární rešerše na dané téma 2. Příprava materiálů pro elektroreologické suspenze 3. Měření dielektrických, elektrických a reologických vlastností elektroreologických suspenzí 4. Vyhodnocení a interpretace dosažených výsledků

Rozsah práce:

Rozsah příloh:

Forma zpracování diplomové práce: **tištěná/elektronická**

Seznam odborné literatury:

1.T.HAO,Electrorheological fluids:The non aqueous suspensions,1st ed.,Cambridge,Massachusetts,2005,ISBN-13: 978-0-4444-52180-4
2.F.KREMER,A.SCHÖNHALS(Eds.),Broadband Dielectric Spectroscopy,Berlin,Germany,2003,ISBN 3-540-43407-0

Vedoucí diplomové práce: **doc. Dr. Ing. Vladimír Pavlínek**
Centrum polymerních materiálů

Datum zadání diplomové práce: **11. února 2009**

Termín odevzdání diplomové práce: **15. května 2009**

Ve Zlíně dne 11. února 2009

doc. Ing. Petr Hlaváček, CSc.
děkan

L.S.

UNIVERZITA TOMÁŠE BATI VE ZLÍNĚ
Fakulta technologická

doc. Ing. Roman Čermák, Ph.D.
vedoucí katedry

ABSTRAKT

Tato diplomová práce je zaměřena na přípravu core-shell kompositních materiálů a hodnocení elektroreologických, dielektrických a elektrických vlastností jejich suspenzí v silikonovém oleji. Titanátové nanotyčinky byly připraveny jako nosič (core). Na povrch nanotyčinek byl v různých koncetracích napolymerován polypyrol (shell). Měření reologických, elektrických a dielektrických vlastností suspenzí potvrdilo, že použitím polypyrolu lze modifikovat vlastnosti titanátových nanotyčinek tak, že došlo k výraznému zvýšení elektroreologického efektu u elektroreologických suspenzí.

Klíčová slova: core-shell materiály, elektroreologie, reologické a dielektrické vlastnosti.

ABSTRACT

This master thesis is aimed on fabrication of core-shell composites and evaluation of electrorheological, dielectric and electric properties of their suspensions in silicone oil. Titanate nanorods were prepared as a core material. Polypyrrole was polymerized on the surface of nanorods in different amounts. Determination of rheological, electric and dielectric properties showed that with the use of polypyrrole properties of titanate nanorods can be modified and significantly enhanced electrorheological effect in electrorheological suspensions is generated.

Keywords: core-shell materials, electrorheology, rheological and dielectric properties.

ACKNOWLEDGEMENTS

First of all, I would like to thank to my supervisor Assoc. Prof. Vladimír Pavlínek. He created an excellent research environment and gave me a lot of advices and help whenever I was in need.

Another thanks are directed to MSc. Qilin Cheng, Ph.D. He helped me with preparation of materials and gave me valuable advices.

Further, I thank to MSc. Martin Stěnička for his time when he helped me with measurement of rheological and dielectric properties as well.

Additional thanks aim to Assoc. Prof. Anežka Lengálová, who has proofread theoretical part of this thesis.

My final and most sincere acknowledgement go to my family including Žofre, especially my girlfriend Markétka whose support and encouragement helped me for finishing this master thesis.

CONTENTS

INTRODUCTION 9
I. THEORY 10
1 ELECTRORHEOLOGICAL SUSPENSIONS 11
1.1 ELECTRORHEOLOGICAL EFFECT 11
1.1.1 POSITIVE AND NEGATIVE ER EFFECTS 12
1.1.2 ELECTRO-MAGNETO-RHEOLOGICAL EFFECT 14
1.1.3 PHOTO ER EFFECT 15
1.2 PROPERTIES OF SUSPENSIONS 15
1.2.1 RHEOLOGICAL PROPERTIES 15
1.2.2 DIELECTRIC PROPERTIES 18
2 ELECTRORHEOLOGICAL MATERIALS 22
2.1 DISPERSED PHASE 22
2.1.1 INORGANIC MATERIALS 22
2.1.2 ORGANIC MATERIALS 23
2.1.3 CONDUCTIVE POLYMERS 23
2.1.4 CORE-SHELL MATERIALS 25
2.2 CONTINUOUS PHASE 26
3 FACTORS INFLUENCING ELECTRORHEOLOGICAL EFFECT 28
3.1 ELECTRIC FIELD 28
3.1.1 ELECTRIC FIELD STRENGTH 28
3.1.2 FREQUENCY 30
3.2 TEMPERATURE 31
3.3 VOLUME FRACTION 32
3.4 ELECTRODE PATTERNS 33
4 APPLICATIONS 34
4.1 DAMPING DEVICES 34
4.2 TORQUE TRANSMISSION DEVICES 35
4.3 HYDRAULIC VALVES 35
5 AIM OF WORK 37
II. ANALYSIS 38
6 EXPERIMENTAL 39
6.1 PREPARATION OF CORE-SHELL MATERIALS 39

6.1.1 CORE MATERIAL 39
6.1.2 SHELL MATERIAL 40
6.2 PREPARATION OF SUSPENSIONS 42
6.3 ELECTRORHEOLOGICAL MEASUREMENT 42
6.4 CURRENT-VOLTAGE MEASUREMENT 42
6.5 DIELECTRIC MEASUREMENT 43
7 RESULTS AND DISCUSION 44
7.1 MORPHOLOGY OF THE SAMPLES 44
7.2 ELECTRORHEOLOGICAL BEHAVIOR 47
7.3 CURRENT-VOLTAGE CHARACTERISTICS 57
7.4 DIELECTRIC PROPERTIES 62
8 CORRELATION BETWEEN DIELECTRIC, ELECTRIC AND ELECTRORHEOLOGICAL PROPERTIES 65
CONCLUSION 68
BIBLIOGRAPHY 69
LIST OF ABBREVIATIONS 75
LIST OF FIGURES 78
LIST OF TABLES 82

INTRODUCTION

Electrorheological suspensions are special kind of „smart“ materials, which can rapidly and reversibly change their rheological properties upon application of an external electric field in kV/mm. Such phenomenon is called electrorheological effect and was discovered by Winslow in 1947 [1].

Usually electrorheological suspensions consist of polarizable particles dispersed in non-conducting liquid medium. Surface properties of particles as well as their density determine two main aspects of such fluids. Polarizability of particles is crucial for generation of intensive electrorheological effect and matching density controls long term stability of suspensions.

Recently, new types of material, namely core-shell, were introduced as a dispersed phase of electrorheological fluids. Cores of various shapes and sizes can be prepared and suitable shell modifies final properties such as density, electrical conductivity, dielectric constant etc. Tailoring of such materials provides potential to develop highly efficient electrorheological suspensions having acceptable stability [2, 3].

Conducting polymers such as polyaniline and polypyrrole represent suitable shell materials for preparation of core-shell composites. They can be easily synthesized on surface of many substrates providing polarizable layer which can be adjusted to required electric and dielectric properties.

Analysis of electric, dielectric and rheological properties of electrorheological suspensions is necessary and their correlation helps to understand their complex behavior.

I. THEORY

1 ELECTRORHEOLOGICAL SUSPENSIONS

An electrorheological (ER) suspension is a colloidal suspension which contains two phases - dispersed phase and continuous phase. The former is mostly represented by solid particles, the latter is formed by non-aqueous liquid medium [2]. Great importance is attached to these suspensions because of their ability to change properties upon application of an external electric field [4].

For ER suspensions to be applicable in industry, following properties have to be achieved:

1. ER suspension should rapidly revert to the low viscosity state, after removal of external electric field
2. ER suspension must be durable after prolonged usage in engineering devices, with regards to their physical and chemical properties
3. ER suspension must be compatible with the material used in engineering devices
4. ER suspension should exhibit resistance against thermal degradation [5, 6].

1.1 Electrorheological effect

ER effect is defined as a change of rheological properties, such as viscosity, shear stress, and shear modulus, in presence of an external electric field. Rheological properties can both increase or decrease; in all cases, the changes are determined by physical properties of both phases [7]. ER suspensions could exhibit several types of ER effects. From the point of view of change in viscosity, shear stress, and modulus, the positive and negative effects can be distinguished. In the former, rheological properties increase with electrical field strength, in the latter decrease. Special type of positive effect is giant ER effect, where huge columns are created in electric field [8, 9].

ER effects are more often divided according to the sensibility to the type of applied field. Than the electro, magneto, electro-magneto rheological effect and photo effect can be distinguished. In the following text, the basic characteristics of each type are described.

1.1.1 Positive and negative ER effects

As described before, the positive ER effect means that the viscosity and yield stress increase when an external electric field is applied. The enhancement is caused by particle reorganization in suspension. The particles are polarized in electric field and create fibrous structures between electrodes due to an applied electric field and their polarizability. Fig.1 shows the mechanism of the particle movement. In the absence of external electric field particles are dispersed randomly in the suspension. When the electric field is applied particles form chain-like structure perpendicularly to the electrodes. When the shear flow is applied the particles move in the fibrous structures in the flow direction [6]. This ER effect was discovered by Winslow [1].

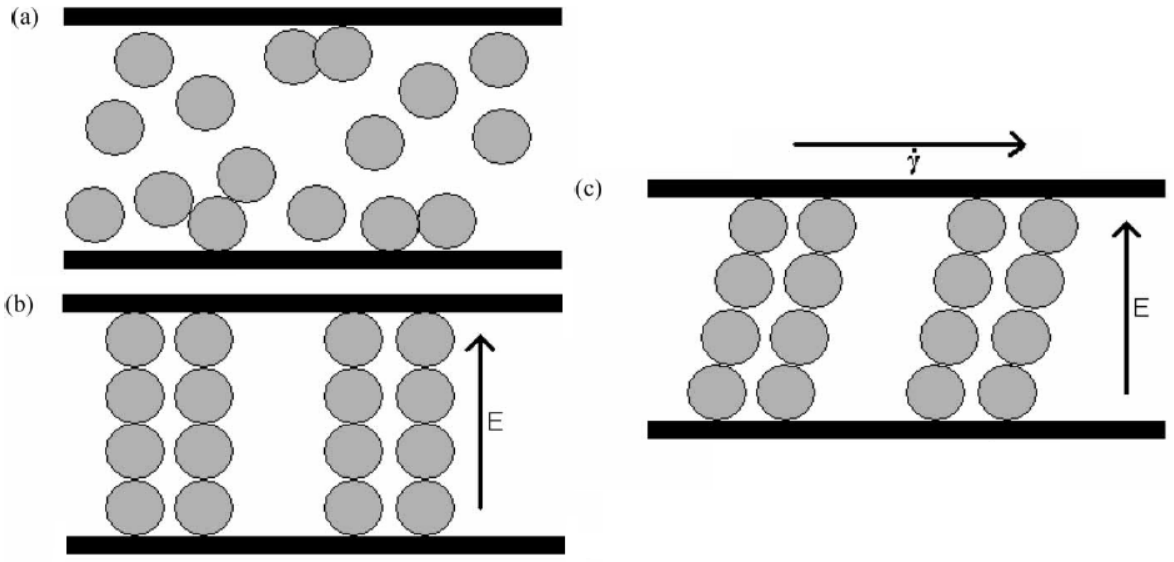

Fig. 1: Schematic diagram of ER suspension (a) without applied external electric field, (b) with applied external electric field, (c) with applied shear flow and external electric field. [6]

Giant ER effect is a special case of positive ER effect and it was recently discovered by Wen [10]. In this case, after application of external electric field, the polarized particles aggregate into columns aligned along the field direction. It was found out that such behavior is attributed to the small size (in order of nanometers) and large surface area and thus high polarizability of the particles, Fig. 3 [11, 12].

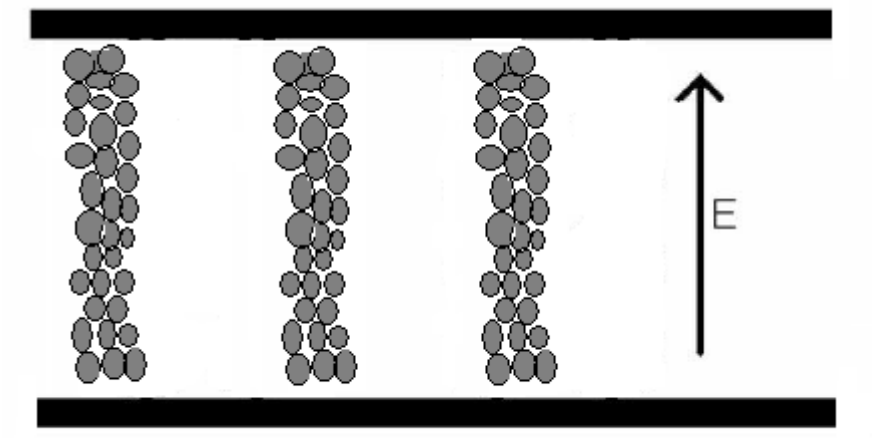

Fig. 2: Schematic diagram of creating columns under applied electric field [11].

Contrary to the positive effect, in the case of the negative ER effect viscosity, shear stress and modulus decrease with increasing external electric field.

As shown in Fig. 3, the particles are either charged nonuniformly, where some particles are negatively charged and some are positively charged (mixed charges) or uniformly (single sign charge). In electric field, particles migrate towards both electrodes. This phenomenon, which is also called electrophoresis, leads to the phase separation in the suspension.

Unlike the positive effect, where chain trough space between electrodes is built, in the case of negative effect, the charges are concentrated at electrodes, what causes decrease in rheological properties with enhancing electric field strength [13].

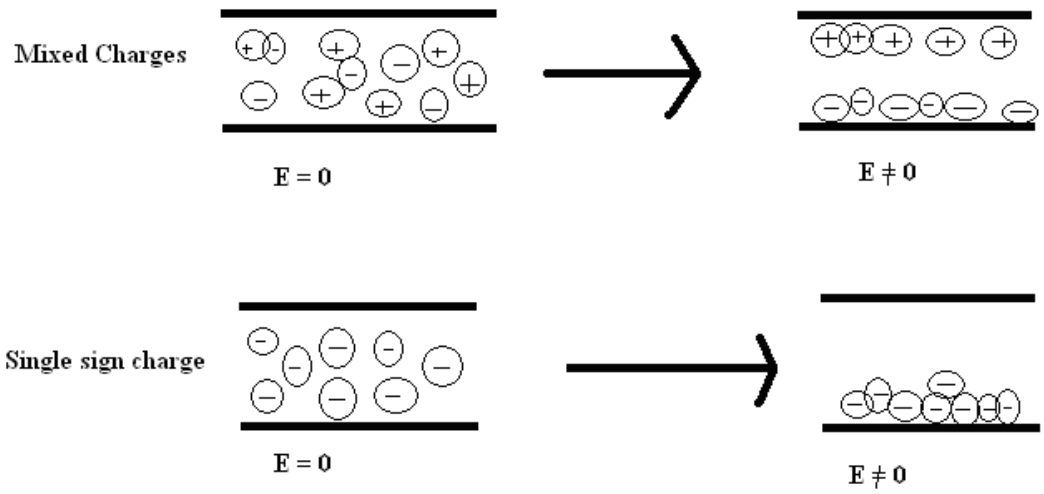

Fig. 3: *Phase separation under an electric field due to electrophoresis, which leads to the negative ER effect [2].*

1.1.2 Electro-magneto-rheological effect

ER effect means that suspensions change their properties in electric field, magnetorheological (MR) effect means that suspension reacts to magnetic field. The combination of both effects is electro-magneto-rheological (EMR) effect. Suspensions could respond to an external electric and a magnetic field separately or simultaneously. Such materials usually exhibit behavior with synergic effect. As shown in Fig.4, the direction of the applied electric field can be parallel or perpendicular to applied magnetic field.

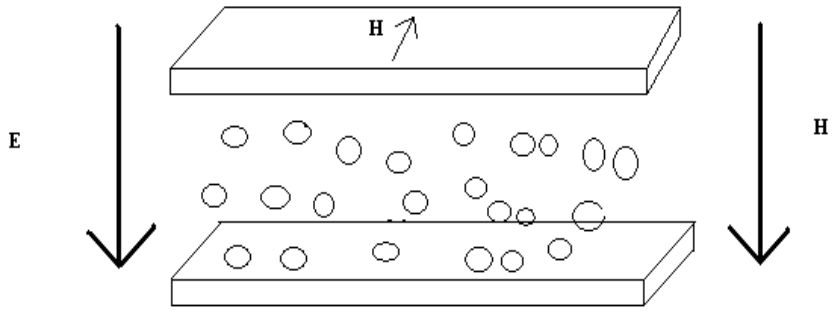

Fig. 4: Schematic illustration of particle organization in EMR effect. H represents applied magnetic field and E represents electric field [2].

The EMR effect is stronger than both ER and MR effects, when electric field alone in the case of ER effect and magnetic field alone is applied in the case of MR effect [14].

1.1.3 Photo ER effect

Photo ER effect is a special type of the ER effect. It was also found out, that the water content is important on the particle surface. It can be easily modified by amount of water in the suspension. Low content (< 2 wt.%) provides positive photo ER effect. When the suspension is illuminated, the low photocurrent appears. Under the influence of electric field, the polarization of the particles creates the chains between the electrodes. The higher content (>3 wt.%) gives negative photo ER effect. When the suspension is illuminated, the photoeletrophoresis occurs under the application of electric field. Particles and their charges are concentrated around both electrodes, which lead to negative photo ER effect [15].

1.2 Properties of suspensions

1.2.1 Rheological properties

Among rheological properties belong shear stress (yield stress), shear viscosity, and shear modulus. In the case of ER suspensions, the rheological properties can be measured either at applied electric field or without electric field. Results are subsequently compared. Values of electric field strength usually lie in interval 0.5-3 kV/mm [1].

In the absence of electric field, the ER suspensions show the Newtonian behavior, when shear stress increases linearly with applied shear rate. This situation is described by following equation.

$$\tau = \eta \cdot \dot{\gamma} \qquad (1)$$

where

τ - shear stress [Pa]

η - shear viscosity [Pa.s]

$\dot{\gamma}$ - shear rate [1/s]

On the other hand, at applied electric field, behavior of ER suspension is changed i.e. viscosity and shear stress increase. Under these conditions, behavior of ER suspensions can be often described by Bingham equation [16, 17].

$$\tau = \eta_P \dot{\gamma} + \tau_y \qquad (2)$$

where

τ – shear stress [Pa]

η_P – plastic viscosity [Pa.s]

$\dot{\gamma}$ - shear rate [1/s]

τ_y – yield stress [Pa]

Fig. 5 shows the typical rheological behavior of ER suspensions. Without an applied electric field the suspension exhibits the linear Newtonian dependence. When the electric field is applied, shear stress reaches plateau at low shear rates [18]. The forces between particles induced by external electric field are higher than hydrodynamic forces generated by shearing. At high shear rates the electrostatic forces are exceeded and hydrodynamic forces are dominant. So that, the shear stress increases with the increasing shear rate [19].

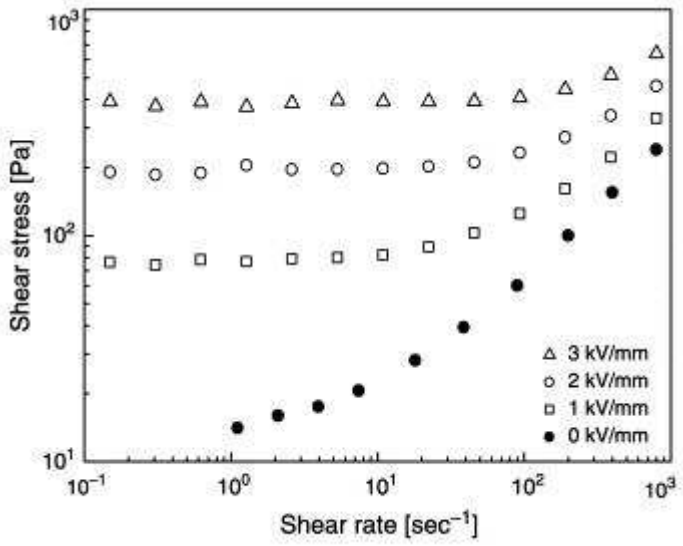

Fig. 5: *Dependence between shear stress and shear rate for poly (napthalene quinone) radical (PNQR) in silicone oil at various electric field strengths [18].*

On the other hand, the higher shearing leads in decreasing viscosity, due to destruction of the chains created in the suspensions, by application of electric field, as can be seen in Fig. 6 [15].

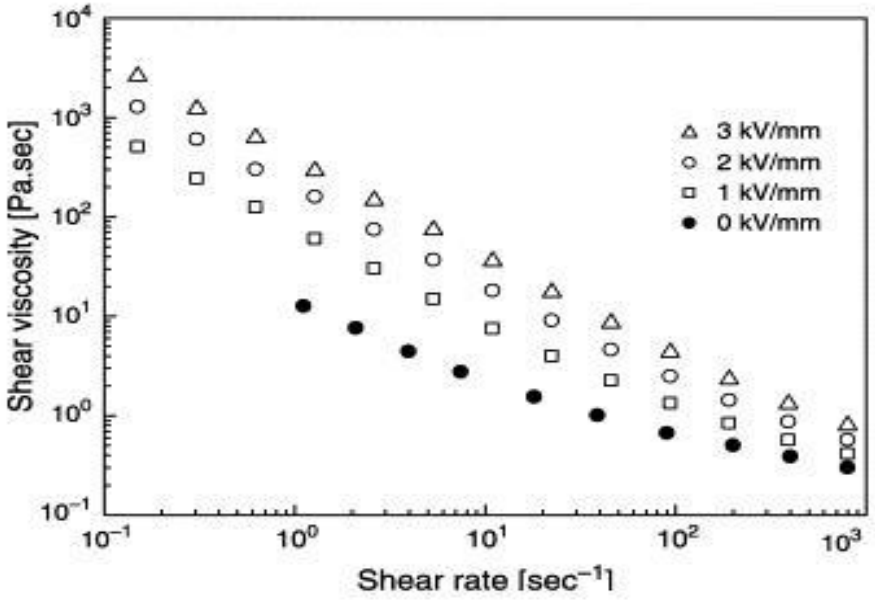

Fig. 6: *Dependence between shear viscosity and shear rate for poly (naphthalene quinone) radical (PNQR) in silicone oil under four various electric field strengths [18]*.

1.2.2 Dielectric properties

Dielectrics are special types of materials, which are able to be polarized, and thus transfer electric charge, in applied electric field. There are several types of polarization such as electronic, atomic, ionic, Debye and interfacial. In the case of ER suspensions, the interfacial polarization mostly occurs. It results from interfaces between the dispersed phase and continuous phase, which have different conductivities. The charge carriers may be trapped at the interfaces, forming the space charge and generating the polarization also called Wagner – Maxwell [6].

Device for measurement of dielectric properties is schematically shown in Fig 7. Material is placed between two electrodes. The net charge is generated on the surface of electrodes [17].

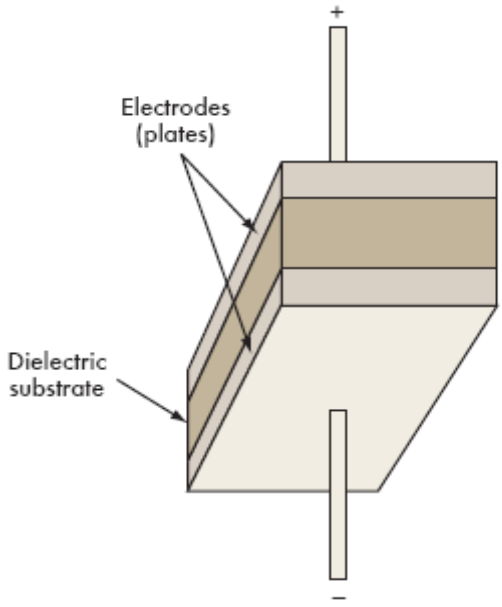

Fig. 7: *Schematic illustration of a dielectric between two electrodes [20].*

Polarization is a time dependent process because dipoles need time to order according to changes in electric field direction.

The ability of a material to become polarized in response to the electric field is controlled by its dielectric constant ε. It could be determined, as a capacitance of condenser with the dielectric between electrodes divided by the capacitance of empty condenser filled with air.

$$\varepsilon' = \frac{C}{C_0} \tag{3}$$

where

ε' – dielectric constant

C_0 – capacitance of empty condenser filled with air

C – capacitance of condenser with the dielectric between electrodes

In the alternating current, dielectric properties depend on the frequency, and are expressed by complex dielectric constant in equation (4).

$$\varepsilon^{*}(\omega) = \varepsilon'(\omega) - i\varepsilon''(\omega) \tag{4}$$

$$\varepsilon' = |\varepsilon| \cos \delta_E \qquad \varepsilon'' = |\varepsilon| \sin \delta_E \tag{5}$$

$$\tan \delta = \frac{\varepsilon''}{\varepsilon'} \tag{6}$$

where

ε^{*} - complex dielectric constant

ε' - dielectric constant

ε'' - dielectric loss factor

tan δ – dielectric loss tangent [20].

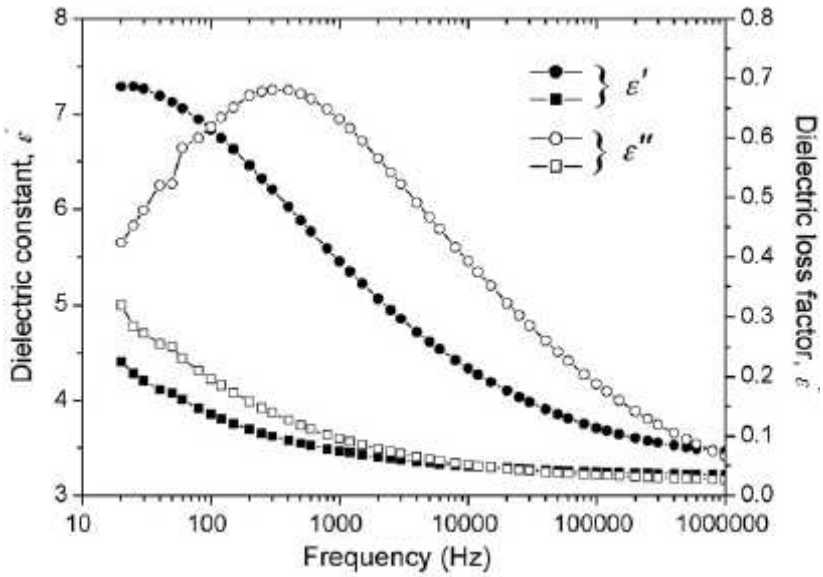

Fig. 8: *Dielectric spectra of electrorheological materials (Na-titanate nanotube (circle points) and H-titanate nanotube (square points)) [19].*

Dielectric properties of the particles such as dielectric constant, ε', dielectric loss factor, ε'', dielectric loss tangent, tan δ, particle polarizability $\Delta\varepsilon$ (eq. 7) and relaxation time, t_{rel} , were presented. Hao [2] experimentally and theoretically determined that the dielectric loss tangent should be higher than 0.1 for good ER activity. Also the polarizability of particles should be large. Therefore the particles are easily polarized and easily create the chains between electrodes. [21] It is required, that the particles should have position of maximum ε'' in a frequency range approximately 10^2-10^5 Hz providing relaxation time short enough. When the relaxation time is low, and electric field is applied, the particles become polarized very quickly. [22]

$$\Delta\varepsilon = \left(\varepsilon'_s - \varepsilon'_\infty\right) \tag{7}$$

where

ε'_s – static dielectric constant

ε'_∞ - high frequency limit dielectric constant

2 ELECTRORHEOLOGICAL MATERIALS

The ER suspensions include dispersed phase and continuous phase. These materials should exhibit some key properties, as already mentioned.

Various types of materials can be used for preparation of such suspensions. In this chapter, materials with advanced properties and usage in ER suspensions are introduced.

2.1 Dispersed phase

The dispersed phase is mostly presented by solid particles [2]. These particles should exhibit following properties.

1. Particle size should be normally in the range 0.1 - 100 μm.
2. The particles creating agglomerates should be ground into the powder before usage.
3. Particles should show minimal sedimentation in the suspensions.
4. Particles should exhibit large polarization under an applied external electric field, leading to strong interparticle forces and a high field induced viscosity.

Particles should be able to polarize in electric field. Polarization means that a charge is formed on the originally electrically neutral particles. These polarized particles create dipoles on their surface and react with external electrical field by movement according to the changes in electric field direction [23].

The size of the particles is significant factor influencing ER properties. Too small particles exhibit high Brownian motion, and thus destroying chains. On the other hand, with increasing particle size, the sedimentation accelerates, which negatively influences forming chains between the electrodes. [24] Hence, too large particles make ER effect weaken.

2.1.1 Inorganic materials

Inorganic particles such as TiO_2, $BaTiO_3$, silica, zeolite, etc. [13, 21, 25, 26] were usually used in ER suspensions and exhibit good ER behavior, due to the small amount of moisture

appeared on the particle surface. On the other hand, these particles prove enhanced sedimentation, which makes the suspension unstable. Another disadvantage is their abrasiveness in ER devices. Also when the higher temperature is applied, water can evaporate and ER effect becomes weaker [2].

2.1.2 Organic materials

Organic materials i.e. potato starch, chitosan, cellulose and its derivates, were also tested in ER suspensions [27, 28, 29, 30]. Comparing to inorganic materials they exhibit lower density and abrasiveness. However they usually absorb large portion of water which makes their properties thermally unstable.

2.1.3 Conductive polymers

Conductive polymers, such as polyaniline (PANI) or polypyrrole (PPy), are often used in ER suspensions [23 31]. PANI is applied due to its thermal stability and lower density than other ER materials. Opposite to inorganics, PANI reduces the problem with the sedimentation. PANI is also often employed for easy preparation by oxidative polymerization as shown in Fig. 9 [32].

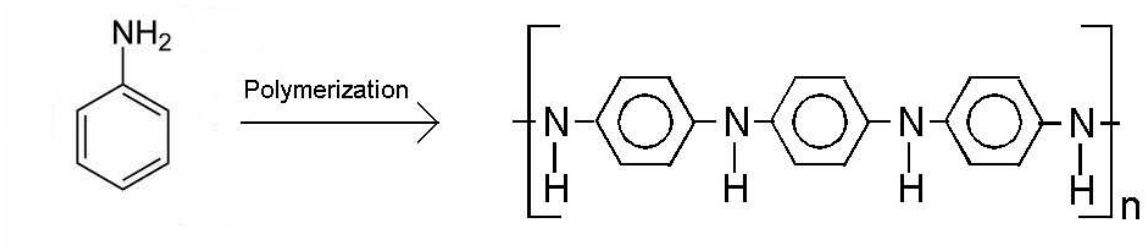

Fig. 9: *Molecular structure of polyaniline [2]*

Conductivity of PANI suitable for preparation of effective ER suspensions can be adjusted by doping process using various acids. Then intensity of ER effect significantly changes with doping level as can be seen in Fig.10. [33]

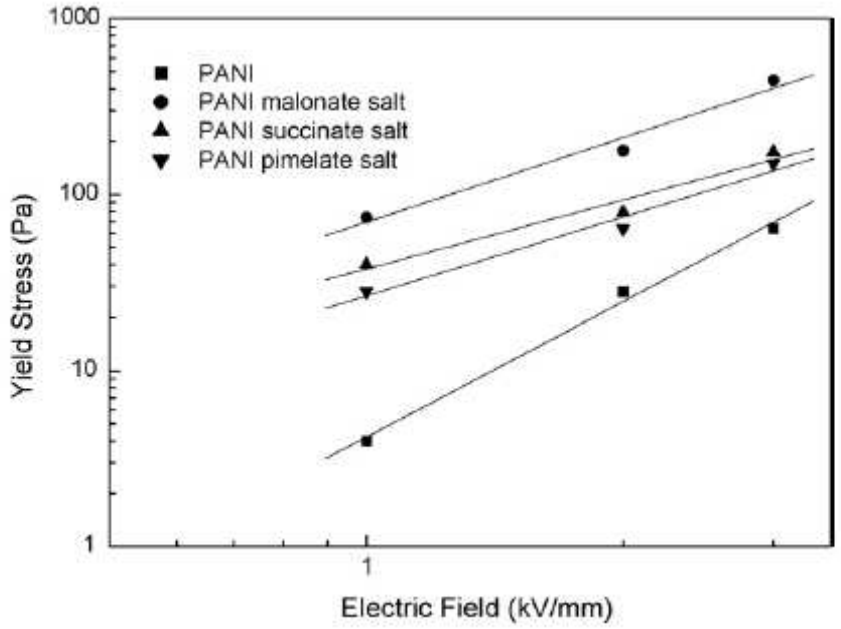

Fig. 10: *Dependence between yield stress and electric field strength. [33]*

Another often employed conductive polymer is polypyrrole (PPy). Angeli and Alessandri in 1916 found out polymerization of pyrrole in acidic atmosphere using H_2O_2 [55] Properties of polypyrrole depend on fabrication and state in which is the polymer. In oxidized state the PPy have a metal character and behave as a conductor. In the neutral state it behaves as a semiconductor and exhibits sufficient conductivity, appropriate density and environmental stability in comparison to many others semiconducting polymers. Suitable conductivity ensures good ER effect and could be adjusted by conditions during polymerization, or by alkalization of the fabricated particles. PPy can be easily prepared by oxidative polymerization, as can be seen in Fig.11. [34]

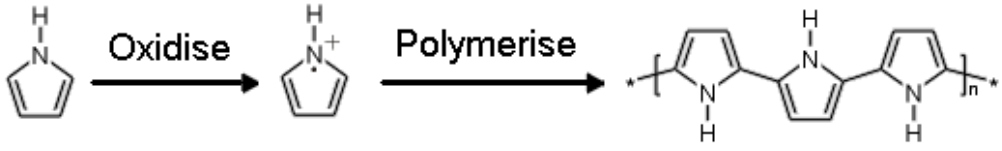

Fig. 11: *Molecular structure of polypyrrole [2]*

It is often used in ER suspensions due to enhanced ER effect. Fig.12 shows, when the higher content of polypyrrole is used in suspension, the ER properties such as yield stress increase. [35] This polymer is applied in core-shell composites as a shell material and exhibits improvement of ER properties.

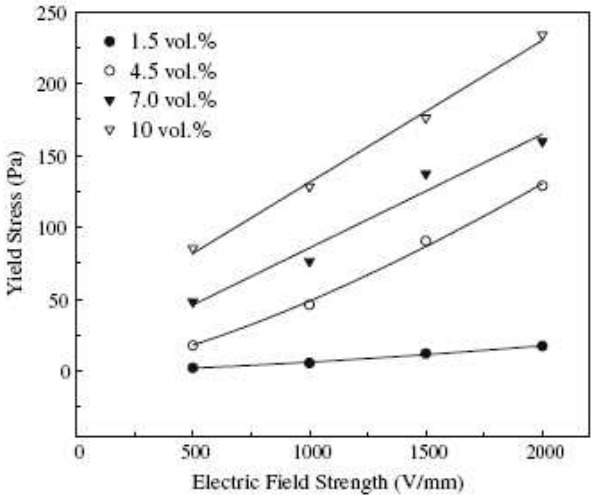

Fig. 12: *Dependence between yield stress and electric field strength at various content of polypyrrole [36].*

2.1.4 Core-shell materials

Core-shell particles are new group of progressive materials used for ER suspensions. The core-shell particle is formed from hard core and soft shell. Materials with high dielectric constant and reasonable conductivity (10^{-8} S/cm) i.e. BaTiO $(C_2O_4)_2$, multiwall carbon nanotubes (MWCNT), titanate nanorods and nanotubes, silica, etc., are frequently used as a core. [8] As a shell material, both polymers and also inorganic materials can be used. Conductive polymers or urea coatings are often employed [10, 11 31, 37,38].

The core-shell materials exhibit enhanced ER effect [12]. ER properties are improved comparing to use of individual components in ER suspensions [2, 38]. As seen in Fig. 13,

the higher the shell content, the higher yield stress. Density of such materials can better match density of continuous phase and thus improve ER suspension stability. [11] This kind of materials have attracted research activities and results show their great potential in design of ER suspensions with high efficiency [39].

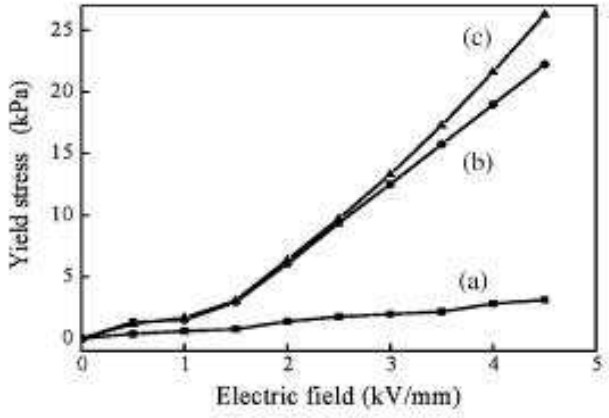

Fig. 13: *Dependence of static yield stress against intensity of electric field of Ba-TiO($(C_2O_4)NH_2CONH_2$) particles in silicone oil (a) sample with least shell content, (b) sample with medium shell content, (c) sample with higher shell content [22]*.

2.2 Continuous phase

As a continuous phase, non-conductive liquids are mostly employed. Water was also tested, but it proved many disadvantages i.e. corrosion, and low range of usage due to low thermal stability. Therefore non-aqueous systems such as mineral or vegetable oils are used at present [2].

Also continuous phase have to reach some important properties:

1. to have a high boiling point and solidifying point (not to be evaporated easily in working temperature range)
2. to have a low viscosity for keeping viscosity of whole suspension at low level at zero electric field
3. to have high resistance and high breakdown strength
4. to have a suitable density
5. to have a high chemical stability (be resistant against degradation and would not react with another materials
6. to have a certain hydrophobicity (would not absorb too much moisture form environment)
7. to have a low toxicity and low cost [17].

Continuous phase has a strong impact on ER effect. Besides suitable density and viscosity, it is important to ensure optimal dielectric constant ratio of particles to the continuous phase. The high dielectric constant value of continuous phase makes the ER effect weaker [40].

Another research explains that the interactions between silicone oil and solid nanoparticles exhibit the significant influence on the ER effect. Results indicate that hydrogen bonds are subservient to linking the silicone oil to ER solid particles. An optimal oil structure, with hydroxyl-terminated silicone oil and a suitable viscosity, could finally create the highest yield stress [24].

3 FACTORS INFLUENCING ELECTRORHEOLOGICAL EFFECT

There are some factors, which could positively or negatively influence the ER effect. The most important factors are electric field - strength and frequency, but also temperature, volume fraction and electrode patterns are crucial to ER behavior.

3.1 Electric field

3.1.1 Electric field strength

The ER effect is induced by external electric field. This effect could not start, until the applied electric field exceeds critical field strength. This value could be expressed as:

$$E_c = \frac{\rho - c}{|\alpha|} \cdot \sqrt{\frac{8\pi k_B T}{c\rho \bar{v} \varepsilon_m}} \quad , \tag{8}$$

where ρ is particle density, c is particle concentration, $\bar{v}$ is the average volume of a particle, k_BT is the thermal energy, ε_m is the dielectric constant of continuous phase. α is a constant expressed as :

$$\alpha = \frac{g}{g + \frac{\varepsilon_m}{(\varepsilon_p - \varepsilon_m)}} \tag{9}$$

where ε_p is the dielectric constant of particles and g is a numerical constant depending on the particle geometry.

Equation (8) indicates that the critical electric field strength decreases with increasing particle concentration. It was experimentally confirmed that the critical electric field

strength is a function of the particle volume fraction, dielectric constant and conductivity of the particles and continuous phase [2].

As can be seen in Fig.14, with increasing electric field strength, polarization between particles increases, hence electric field viscosity increases.

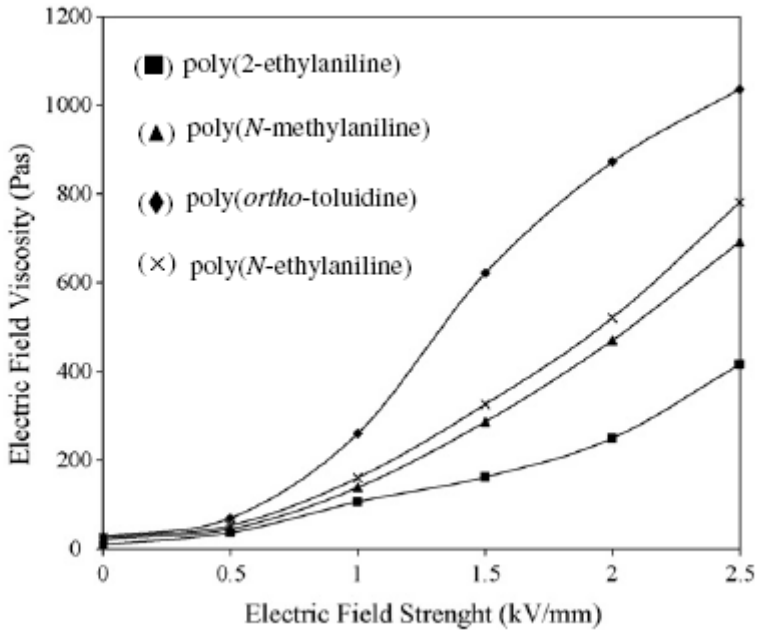

Fig. 14: Dependence between electric field strength and electric field viscosity of various polyaniline derivates [41].

The shear stress - external electric field dependence is plotted in Fig.15. Shear stress is usually proportional to square of electric field strength E^2. This trend originates from the stronger interactions between particles induced by electric field strength [41].

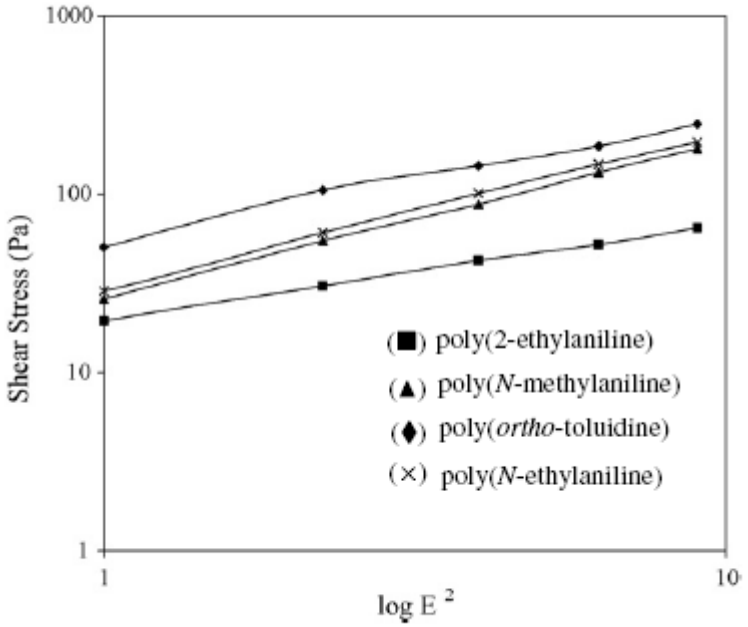

Fig. 15: Dependence between shear stress and external electric field of various polyaniline derivates [41].

3.1.2 Frequency

Frequency plays important role in ER suspensions applications. ER suspensions behave in a different way at low and high frequencies. At low frequencies, polarized particles move according changes of electric field direction, and line up perpendicular to the electrodes. On the other hand, at high frequencies, the polarized particles are not able to respond to the electric field. Therefore polarization can be only occurred through the molecular orientation, Fig.16 [42]. At frequency 200 Hz, field induced change in the shear stress $\Delta\tau$ decreases with frequency. Around the 10 kHz, the value of $\Delta\tau$ is almost zero, which can be interpreted, due to relaxation effect of induced polarization [43].

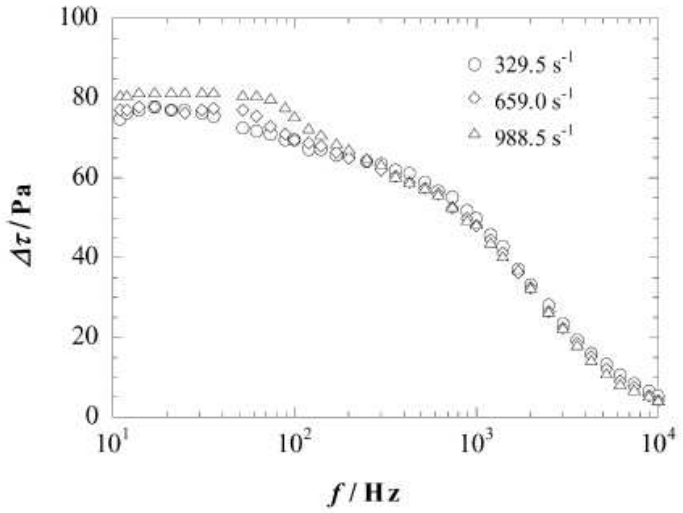

Fig. 16: *Shear stress vs. frequency of the electric field (1 kV/mm) at various shear rates [42].*

3.2 Temperature

There are two approaches to explain the impact of temperature on ER effect. The former is that temperature changes polarizability of the ER suspensions. Because of the higher temperature the dielectric properties and particle conductivity are changed.

The latter is that temperature influences the particle thermal motion. At the higher temperature, the Brownian motion is intensive and particles could not create the fibrillated structures inside the suspension and ER effect becomes weaker.[2]

As can be seen in Fig.17, the shear stress increases with raising temperature. At lower temperatures particles cannot move through suspension and hardly creates the chains between electrodes. When the temperature raises the viscosity of the suspension decreases, hence the particles can easily form the chains perpendicular to the electrodes. On the other hand, when the temperature is too high, Brownian thermal motion is intensified which leads to lower stability of suspension [44].

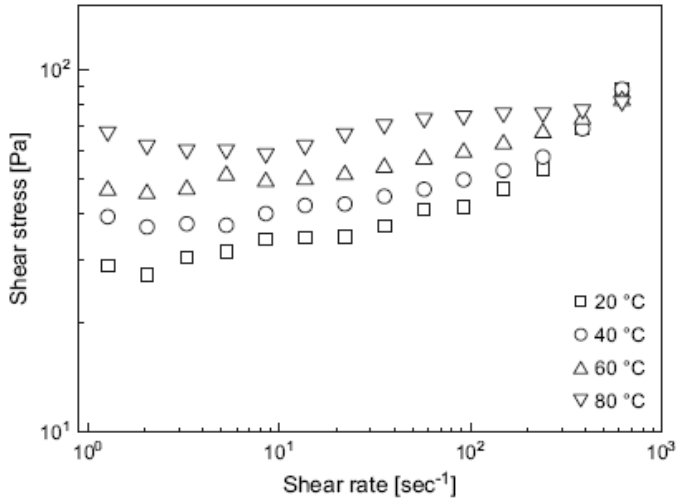

Fig. 17: Dependence between shear stress and shear rate of DBSA-doped PANI based ER suspension at various temperatures [44].

3.3 Volume fraction

The particle volume fraction influences rheological properties. As seen in Fig. 18 yield stress increases with increasing particle volume fraction [45].

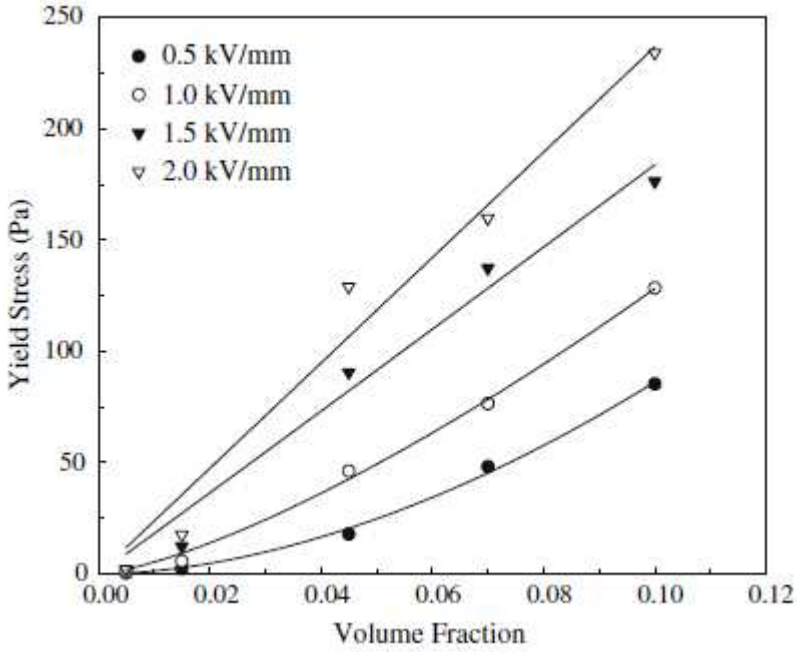

Fig. 18: Dependence of yield stress against volume fraction of PPy-SnO_2-methylcelulose nanocomposite suspension at various electric field strengths [30].

It was found out experimentally, that the optimal volume fraction for ER effect is between 5 and 30 %. If the particle volume fraction is out of this range, ER suspensions exhibit insufficient ER activity [46].

3.4 Electrode patterns

The impact of electrode patterns has been discussed in many studies [47, 48, 49]. Samples with electrode surfaces roughened by sandpaper showed higher ER effect than the original one. On the other hand, sample with attached circular or rectangular polyvinyl patches on the electrode surfaces did not significantly show a difference from the original one [50]. Another group found out [51] that the induced changes in the local electric field, resulted in a highly localized structure on the electrode with axial grooves and ridges. The measured stress was twofold higher comparing to the smooth electrode. Also the coating by polyethylene glycol terephthalate (PETG) mesh increases the ER effect [52].

4 APPLICATIONS

Electrorheological suspensions are advanced in many industrial areas. ER effect enables continuously and reversibly change mechanical strength of ER suspensions from liquid state to the solid state by simply adjusting the properties of external electric field. This phenomenon has been applied in various devices, such as damping devices, torque transmission devices, hydraulic waves and many others [1].

4.1 Damping devices

Damping devices ensure conversion of mechanical energy into thermal energy. They can be categorized as flow mode, shear mode, or mixed mode devices. Flow mode devices employ a pseudo-Poiseuille or pressure flow of ER materials, and the electrified flow boundaries are stationary with respect to the flow. Shear mode devices employ a pseudo-Couette flow of ER material, and one electrified flow boundary moves with respect to the flow. Mixed mode devices employ a combination of both shearing and channel flow. Fig.19 presents three dampers employing the flow mode, mixed mode, and shear mode in ER dampers. In these devices, control of the electric field across the ER flow modulates the force that opposes the motion of the plunger.

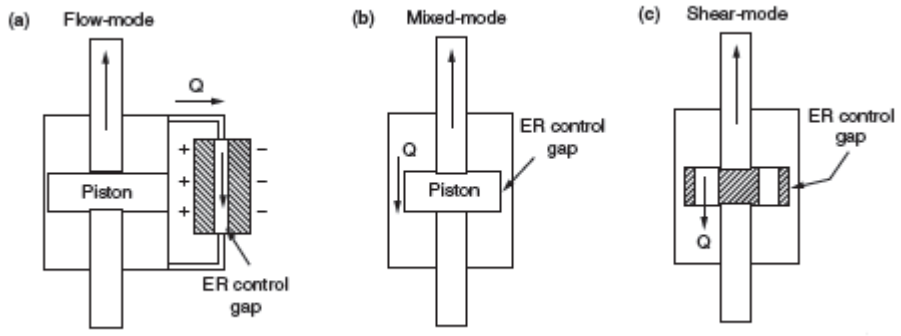

Fig. 19: Illustration of three operating modes in ER dampers [53].

4.2 Torque transmission devices

Very important area of application of ER fluids include transferring and controlling torque from a power source or engine to any number of devices as shown in Fig. 20. This device is currently used like torque converters and friction clutches in automobiles and other types of magnetic or centrifugal clutches for less severe applications such as automobile air conditioners. Such devices present potential of very simple machines with direct computer control.

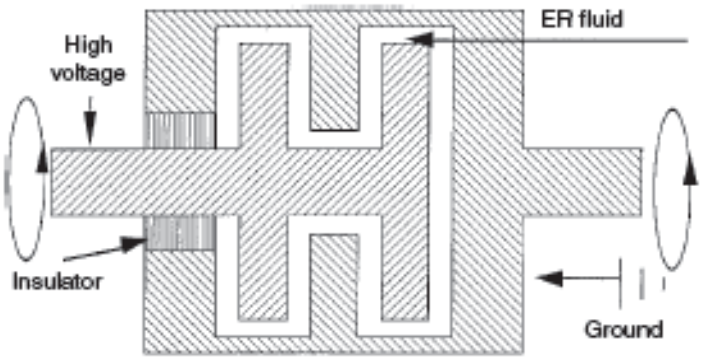

Fig. 20: Illustration of two clutches includes two plates or rotors [53].

4.3 Hydraulic valves

ER valves could modulate flows continuously from full open to full shut, would be much smaller, much faster, require much less power, and could be controlled directly by computer. The primary control parameters in hydraulic circuits are pressure and volumetric flow rate. The ER valve in a hydraulic channel circuit is schematically shown in Fig. 21 [53].

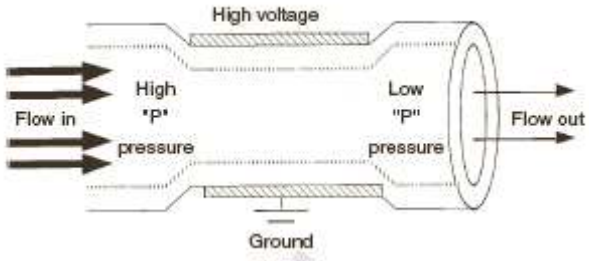

Fig. 21: The ER valve with electrodes on the both sides of the tube trough which ER active suspension flows [53].

There are many others application where the ER suspensions are used i.e. gripping devices, seismic controlling frame structure, and human muscle stimulator. These materials have a various applications and have vast industrial needs [54].

5 AIM OF WORK

The aims of the Master Thesis are as follows:

- Selection of suitable core and shell materials for preparation of composites.
- Preparation of samples with different amount of shell content.
- Determination of rheological and dielectric properties.
- Evaluation of obtained results.

II. ANALYSIS

6 EXPERIMENTAL

6.1 Preparation of core-shell materials

6.1.1 Core material

Titanate (TNt) nanorods were prepared from TiO_2 nanoparticles by synthesis with following procedure.

1.5 g of TiO_2 nanoparticles was dissolved in 70 ml of 10M NaOH for 5 minutes, then solution was filled in 100 ml autoclave. After that, solution was heated at 200°C for 24 hours. Finally, autoclave was cooled down naturally. Fabricated TNt nanorods (white precipitate) were washed by distilled water several times to neutral pH=7.

Fig. 22: Steel autoclave for preparation of TNt nanorods

Steel autoclave contains container from polytetrafluorethylene (PTFE), providing high thermal and chemical stability and good sealing properties. (Fig. 22)

6.1.2 Shell material

PPy was applied as a shell material on the TNt nanorods. The syntheses of PPy on the nanorods can be also seen at Fig. 24 and were performed in the apparatus shown in Fig. 23.

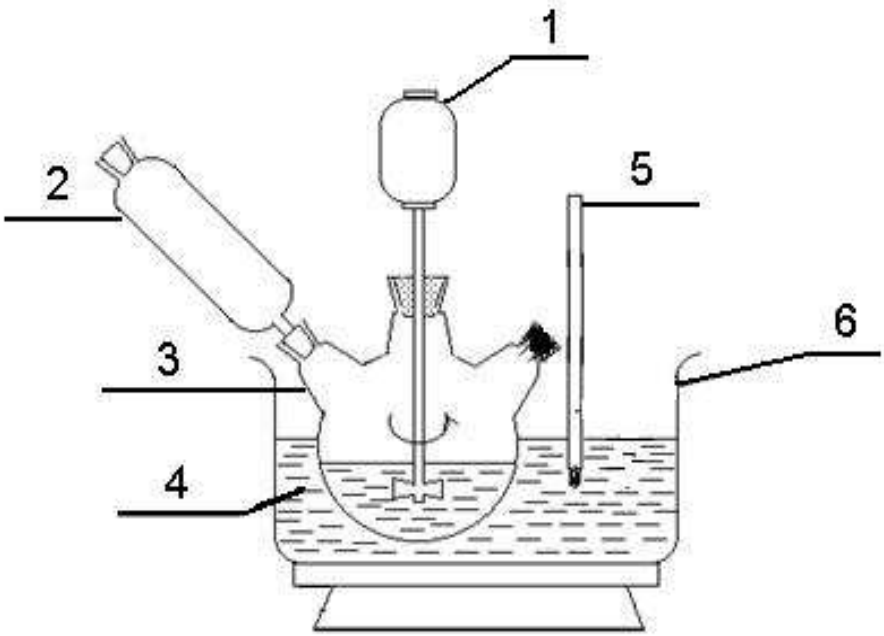

Fig. 23 : Apparatus for preparation of core-shell composites (1 - mixing device, 2 –flask with dropper, 3 – three-necks flask, 4 – cooling medium, 5 – thermometer, 6 – pot)

1.845 g of cetyltrimethylammoniumbromid (CTAB) was dissolved in 100 ml of distilled water. This solution was stirred for 30 minutes. After that, 2 g of TNt nanorods were put into the CTAB solution and sonificated for 20 minutes. Then suspension was transferred into the three-necks flask mixed at 365 rpm and cooled down to 0-5°C. Later, pyrrole (Py) was added into the flask at different amounts. Initiator ammoniumpersulfate (APS) was added into the solution dropwise after another 10 minutes. Composition of samples is shown in table 1.

Table 1: Composition of samples

	TNt nanorods [g]	pyrrole [ml]	ammoniumpersulfate [g]
Sample 1	2.0	0.0	0.00
Sample 2	2.0	0.5	1.64
Sample 3	2.0	1.0	3.32
Sample 4	2.0	2.0	6.64
Sample 5	2.0	4.0	13.28

After addition of initiator, the solution in the three-necks flask was cooled to 0-5°C for 8 hours and another 12 hours kept under room temperature during polymerization. Then the polypyrrole-TNt nanorods were filtered. CTAB was removed from composite by washing with distilled water. All surfactant should be removed because it could have negative impact on electrorheological activity.

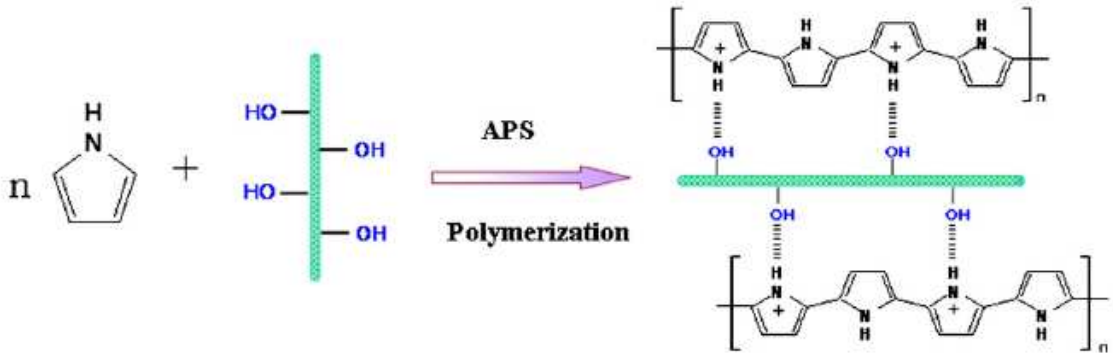

Fig. 24: Schematic formation mechanism for theTNt/PPy composite[56]

In order to decrease conductivity of PPy, prepared samples were put into the flask with 40 ml of 3 vol. % aqueous ammonia and stirred for 12 hours. Then the samples were washed with distilled water to dismiss the aqueous ammonia from the particles and dried in oven for 6 hours at 60°C. This procedure was repeated twice.

Finally, samples were grinded in agate mortar to the fine powder and stored in the plastic polypropylene bottle in desiccator.

6.2 Preparation of suspensions

Samples of prepared core-shell materials and pure TNt nanorods were dried at 80°C for 48 hours under vacuum to ensure that they do not contain moisture.

TNt-polypyrrole composite particles were dispersed in silicone oil (Lukosiol M200, Chemical works Kolín, Czech Republic: η_c = 200 mPa.s, σ_c ~10^{-11}S/cm) to prepare 5 wt.% suspensions. At first, suspensions were stirred mechanically with glass stick and then sonificated for 30 seconds before each experiment.

6.3 Electrorheological measurement

The ER properties were measured with rotational rheometer Bohlin Gemini (Malvern Instruments, UK) with coaxial-cylinders geometry. The rotating inner cylinder of 14 mm in diameter and stationary outer cylinder were separated by 0.7 mm gap. Measurements were carried out at controlled shear rate mode in the range of 0.1 – 300 1/s and DC electric field strengths 0 – 3 kV/mm. The chosen geometry was connected to DC high-voltage source TREK (TREK 668B, USA). All rheological measurements were performed at 25°C.

6.4 Current-voltage measurement

Current-voltage characteristics were measured with the rotational rheometer Bohlin Gemini (Malvern Instruments, UK) with coaxial-cylinders geometry. The rotating inner cylinder of 14 mm in diameter and stationary outer cylinder were separated by 0.7 mm gap. Instrument modified for ER experiments was connected with DC high-voltage source TREK (TREK 668B, USA), digital multimeter (Hexagon 720, Germany) and used for measurement of the time dependence of the current passing through the suspension in the time range of 0-300 s without rotation of inner cylinder. Before each measurement at a new electric field strength the chain created between electrodes were destroyed by shearing the sample at shear rates 20 1/s for 80 s.

6.5 Dielectric measurement

Frequency dependences (in range of 10 – 10^5 Hz) of dielectric constant ε' and dielectric loss factor ε'' of 5 wt% suspensions were measured with Hioki (3522 RCL, Hi Tester, Japan) at 25°C.

7 RESULTS AND DISCUSION

7.1 Morphology of the samples

Morphologies of TNt nanorods and PPy/TNt composites characterized by SEM are shown in Figs. 25-29. TNt nanorods with diameters of about 100 nm and length up to several microns are observed in Fig. 25. The PPy/TNt composites exhibit different morphology than TNt nanorods. Diameter of the nanorods is changed with concentration of pyrrole in the reaction mixture. Average diameter grows with higher content of pyrrole added during polymerization. PPy is obviously polymerized on the surface of TNt nanorods, however PPy forms shell onto the surface of each TNt nanorod as can be seen in Figs. 65-29. Therefore this fibrillar composite has a typical core-shell structure.

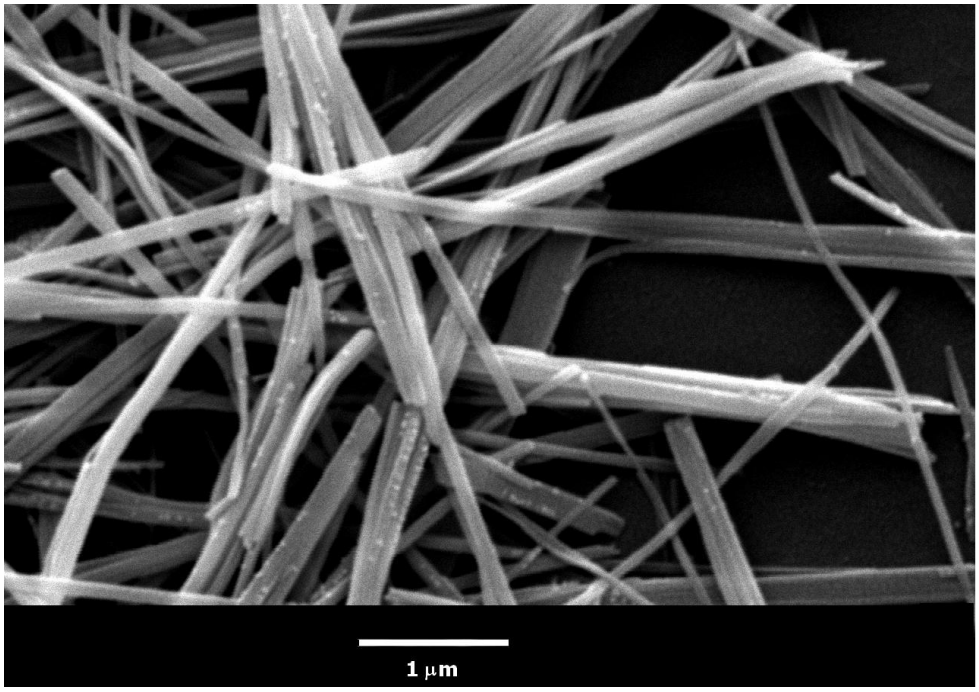

Fig. 25: SEM image of sample 1.

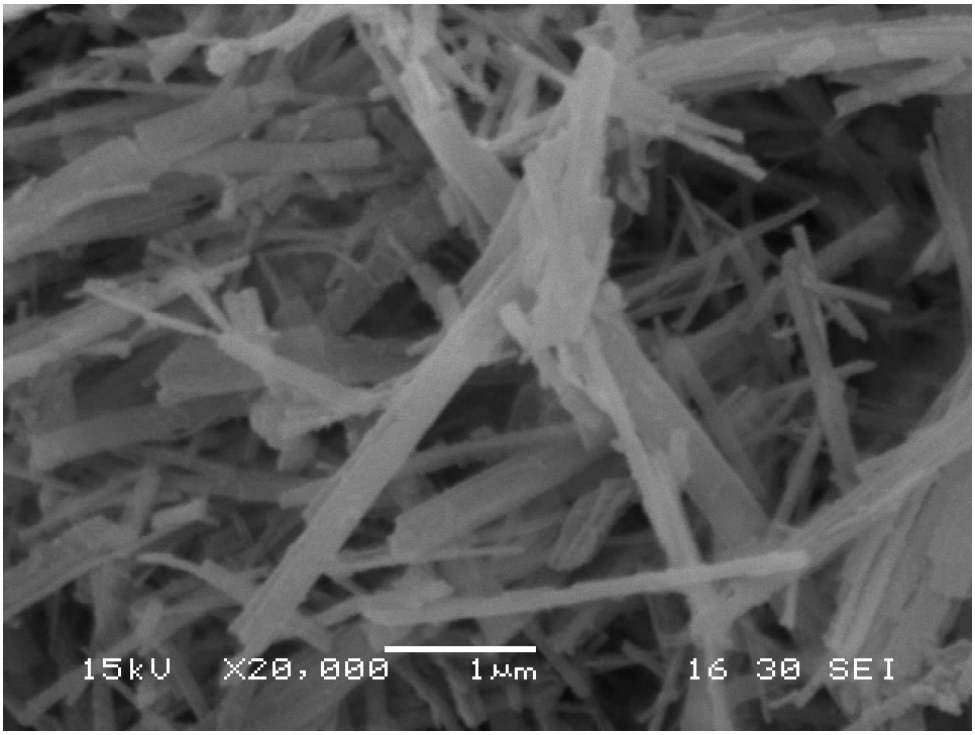

Fig. 26: SEM image of sample 2.

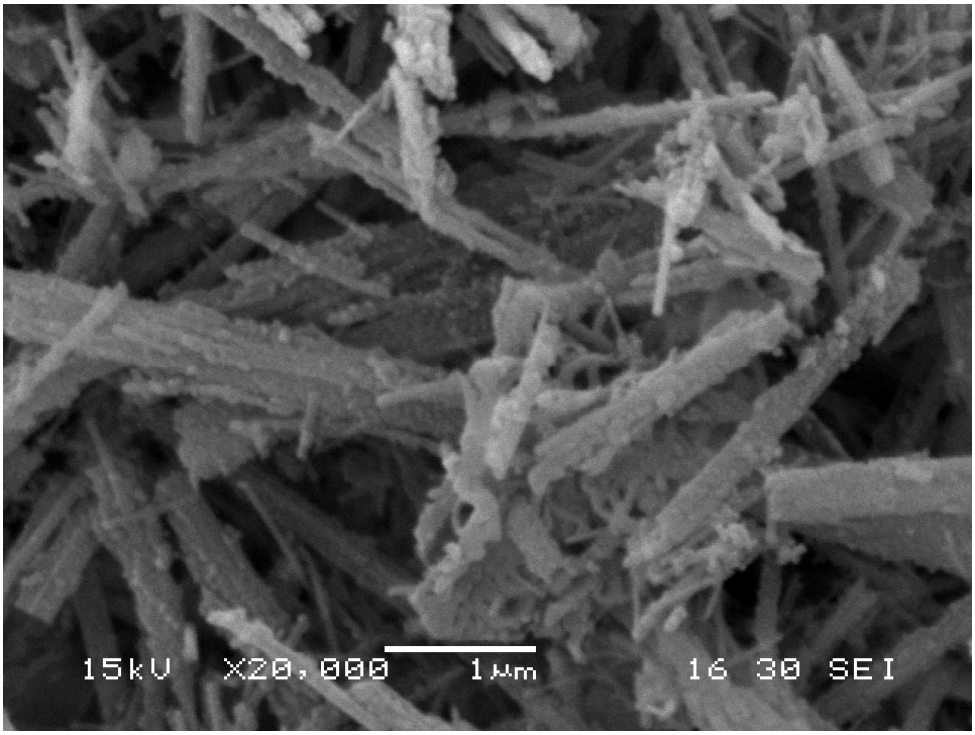

Fig. 27: SEM image of sample 3.

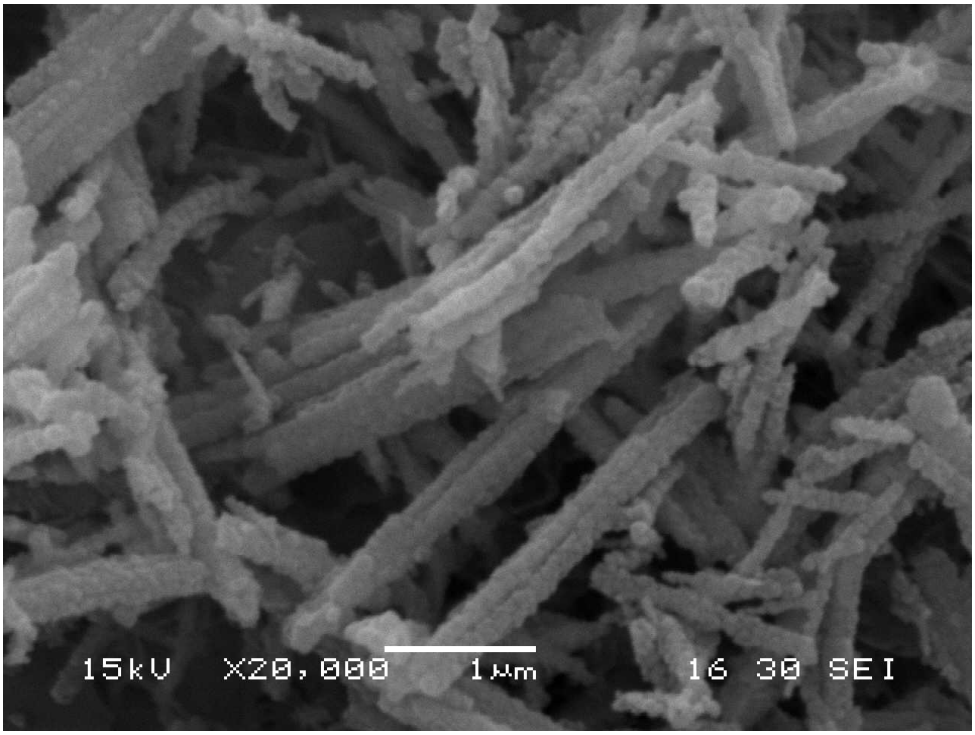

Fig. 28: SEM image of sample 4.

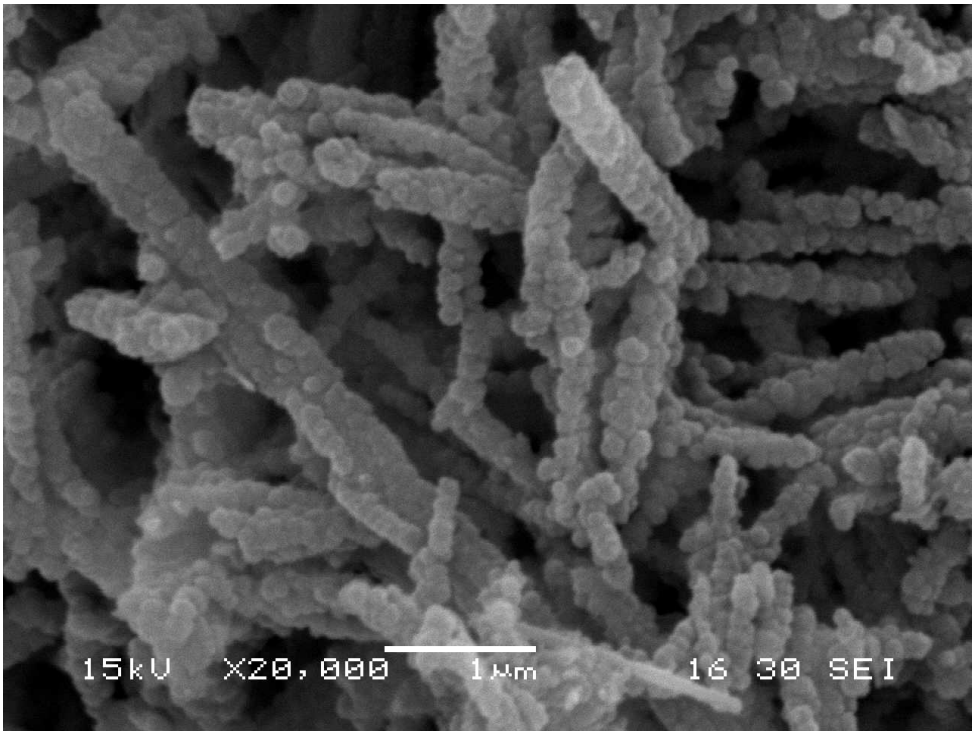

Fig. 29: SEM image of sample 5.

7.2 Electrorheological behavior

Figs. 30-34 show shear stress as a function of shear rate for 5 wt. % suspensions at various electric field strengths. Without an applied electric field shear stress linearly increases with the shear rate and thus the samples exhibit a Newtonian-like behavior. When the electric field is applied suspensions show yield stress as a consequence of created chain-like structures between electrodes. At low shear rates electrostatic forces dominate over hydrodynamic ones due to strong interactions between particles under applied electric field. At higher shear rates, the hydrodynamic forces dominate over electrostatic ones. With increasing shear rates chains are being continuously destroyed and samples exhibit liquid-like behavior.

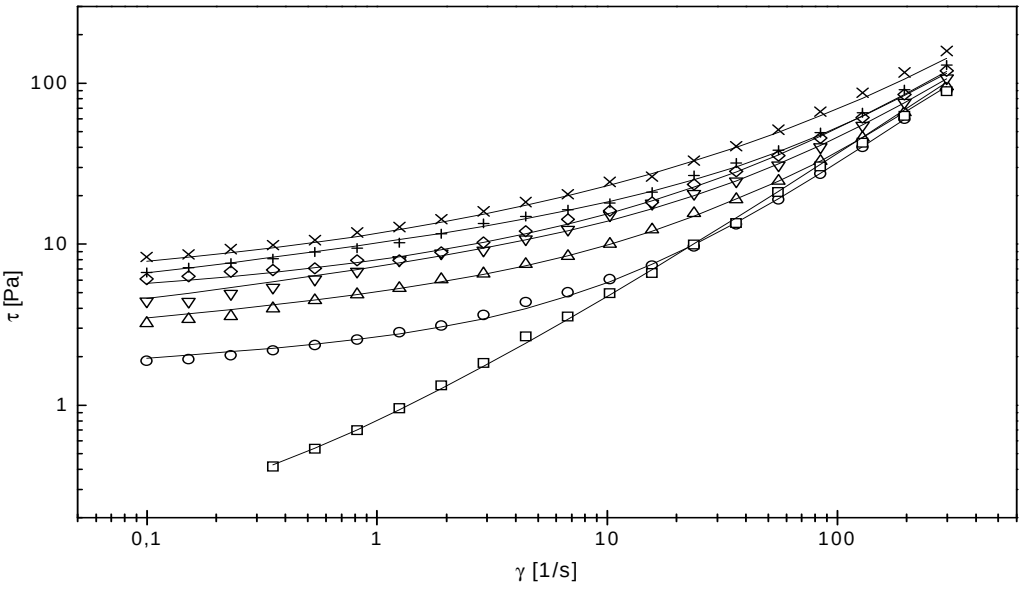

Fig. 30: Dependence of shear stress, τ, on shear rate, γ, for sample 1 at various electric field strengths E (kV/mm): □ 0, ○ 0.5 , ◇ 1.0, △ 1.5, ▽ 2.0, + 2.5, × 3.0. Solid lines represent Choi-Choi-Jhon model fit.

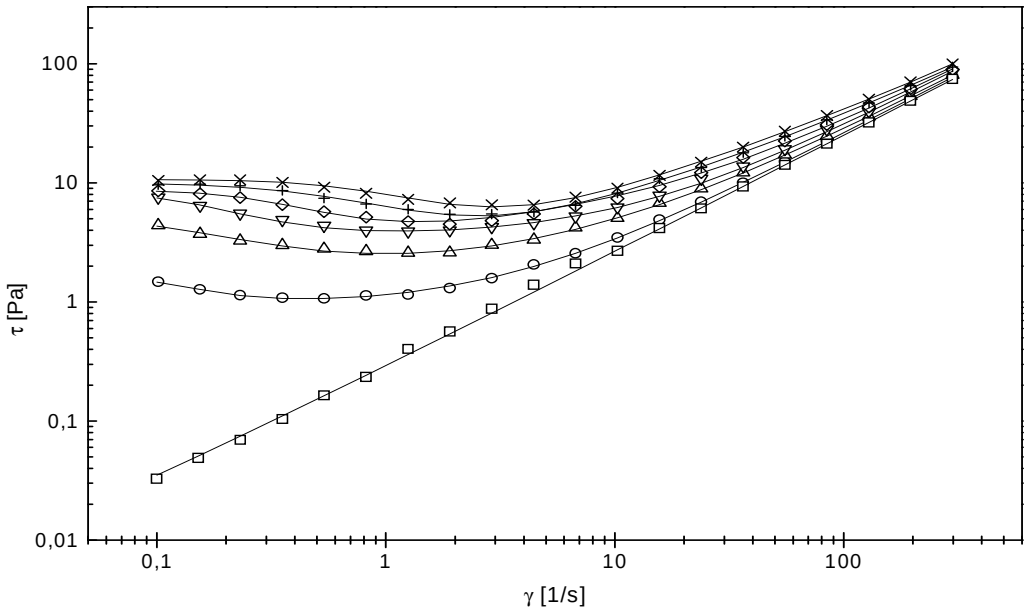

Fig. 31: Dependence of shear stress, τ ,on shear rate, γ, for sample 2 at various electric field strengths E (kV/mm): □ 0, ○ 0.5 , ◇ 1.0, △ 1.5, ▽ 2.0, + 2.5, × 3.0. Solid lines represent Choi-Choi-Jhon model fit.

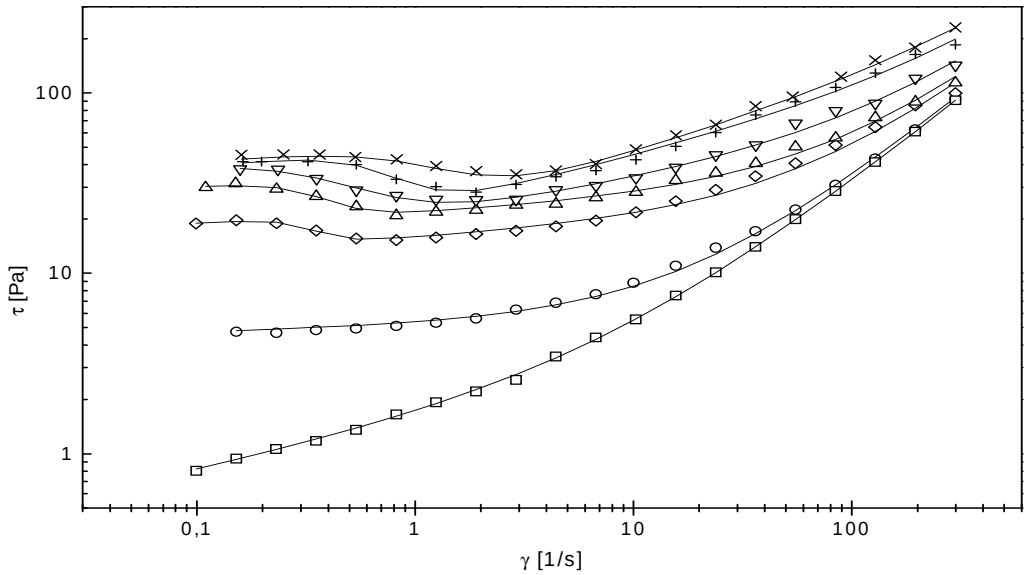

Fig. 32: Dependence of shear stress, τ ,on shear rate, γ, for sample 3 at various electric field strengths E (kV/mm): □ 0, ○ 0.5 , ◇ 1.0, △ 1.5, ▽ 2.0, + 2.5, × 3.0. Solid lines represent Choi-Choi-Jhon model fit.

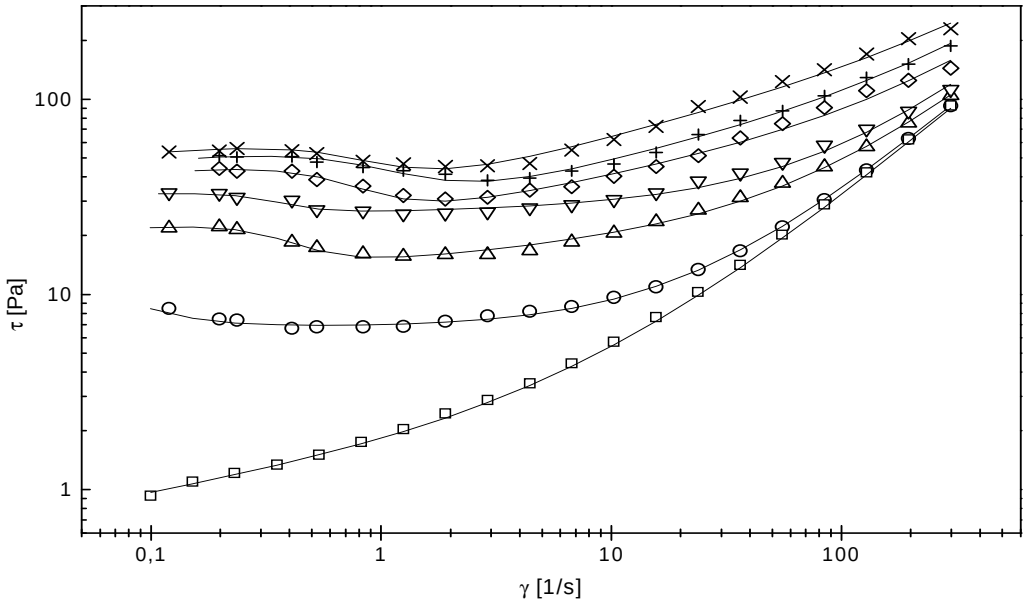

Fig. 33: Dependence of shear stress, τ ,on shear rate, γ, for sample 4 at various electric field strengths E (kV/mm): □ 0, ○ 0.5 , ◇ 1.0, △ 1.5, ▽ 2.0, + 2.5, × 3.0. Solid lines represent Choi-Choi-Jhon model fit.

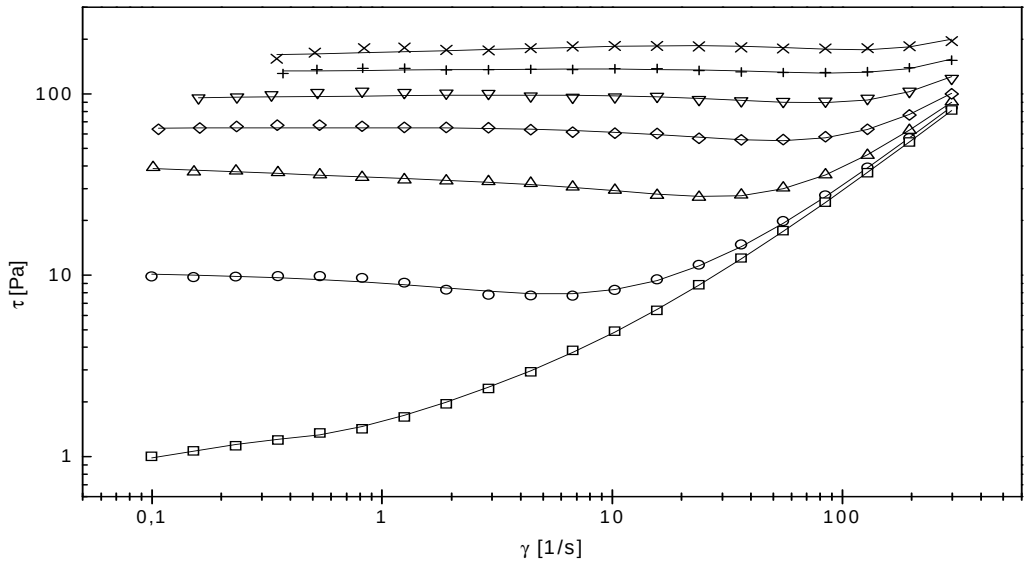

Fig. 34: Dependence of shear stress, τ ,on shear rate, γ, for sample 5 at various electric field strengths E (kV/mm): □ 0, ○ 0.5 , ◇ 1.0, △ 1.5, ▽ 2.0, + 2.5, × 3.0. Solid lines represent Choi-Choi-Jhon model fit.

Electrorheological data including shear stress and shear viscosity were fit by Choi-Choi-Jhon model (eq.10) [19]. Six parameters of this model were determined using least square method in Solver option of MS EXCEL and are shown in tables 2-6.

$$\tau = \frac{\tau_y}{1+\left(t_1 \dot{\gamma}\right)^{\alpha}} + \eta_{\infty}\left(1+\frac{1}{\left(t_2 \dot{\gamma}\right)^{\beta}}\right)\dot{\gamma} \qquad (10)$$

where α is related to decrease in the shear stress, β is exponent and falls $0<\beta<1$, t_1 and t_2 are time constants, and η_{∞} is the shear viscosity at a high shear rate in the absence of an electric field. It is found that this model can describe the stress decrease phenomena at low shear rates region as well as to provide yield stress τ_y.

Table 2: Parameters of the Choi-Choi-Jhon model for sample 1

	0 kV/mm	0.5 kV/mm	1.0 kV/mm	1.5 kV/mm	2.0 kV/mm	2.5 kV/mm	3.0 kV/mm
τ_y	0.13	0.59	1.57	2.18	2.80	3.47	5.03
t_1	0.04	0.63	0.17	0.36	0.46	0.66	0.79
α	40.57	7,78	6.24	5,92	0.89	0.61	0.42
η_{∞}	0.28	0.28	0.28	0.28	0.28	0.28	0.28
t_2	0.36	0.11	0.04	0.02	0.02	0.01	0.001
β	0.33	0.90	0.77	0.78	0.79	0.77	0.67

Table 3: Parameters of the Choi-Choi-Jhon model for sample 2

	0 kV/mm	0.5 kV/mm	1.0 kV/mm	1.5 kV/mm	2.0 kV/mm	2.5 kV/mm	3.0 kV/mm
τ_y	0.01	0.68	4.86	7.24	8.38	9.93	10.14
t_1	6.76	7.35	7.22	3.48	1.76	1.33	0.87
α	4.91	2.61	1.17	1.14	1.20	1.29	1.50
η_∞	0.24	0.26	0.26	0.26	0.24	0.24	0.23
t_2	0.48	0.30	0.11	0.06	0.03	0.02	0.01
β	0.28	0.98	0.89	0.8	0.62	0.57	0.53

Table 4: Parameters of the Choi-Choi-Jhon model for sample 3

	0 kV/mm	0.5 kV/mm	1.0 kV/mm	1.5 kV/mm	2.0 kV/mm	2.5 kV/mm	3.0 kV/mm
τ_y	0.01	3.64	5.87	12.44	26.331	31.804	32.504
t_1	0.48	16.96	2.96	2.67	2.114	1.345	0.818
α	18.43	14.12	5.39	3.86	2.042	2.433	2.063
η_∞	0.28	0.30	0.30	0.30	0.300	0.300	0.300
t_2	0.11	0.05	0.01	0.01	0.005	0.002	0.002
β	0.74	0.96	0.93	0.92	0.808	0.705	0.662

Table 5: Parameters of the Choi-Choi-Jhon model for sample 4

	0 kV/mm	0.5 kV/mm	1.0 kV/mm	1.5 kV/mm	2.0 kV/mm	2.5 kV/mm	3.0 kV/mm
τ_y	0.14	4.21	17.25	22.00	27.101	34.769	36.777
t_1	0.49	12.52	5.19	8.34	1.369	0.951	1.223
α	3,65	2.80	1.80	1.39	2.573	2.056	2.181
η_∞	0.28	0.29	0.27	0.3	0.270	0.280	0.280
t_2	0.11	0.04	0.01	0.01	0.003	0.002	0.001
β	0.76	0.99	0.90	0.94	0.794	0.742	0.716

Table 6: Parameters of the Choi-Choi-Jhon model for sample 5

	0 kV/mm	0.5 kV/mm	1.0 kV/mm	1.5 kV/mm	2.0 kV/mm	2.5 kV/mm	3.0 kV/mm
τ_y	0.21	9.44	18.98	60.79	85.38	120.043	126.867
t_1	2.35	0.15	0.04	0.02	0.01	0.005	0.008
α	3.78	0.52	1.31	0.99	1.08	1.069	1.349
η_∞	0.25	0.28	0.27	0.27	0.27	0.280	0.280
t_2	0.12	0.16	0.03	0.04	0.02	0.011	0.003
β	0.76	0.99	0.95	0.90	0.89	0.886	0.871

TNt nanorods (sample 1) exhibit weak ER effect as can be seen in Fig.30. Shape of the curves indicates that electrostatic forces between particles are not strong. Chains are broken at relatively low shear rates. Nevertheless ER behavior was observed and yield stress increases with increasing electric field strength, and at E = 3.0 kV/mm it reached around 5 Pa.

Samples 2 and 3 in Figs.31 and Fig.32 provided similar behavior. At low shear rates electrostatic forces are strong and thus structure created under an applied external electric field is stiff. Flow curves show local minimum which can be explained as follows. Under critical value of the shear rate electrostatic forces compete with hydrodynamic ones. Above this value hydrodynamic forces dominate and chain-like structure is continuously broken. Suspensions exhibit pseudo-Newtonian behavior. Such a kind of behavior corresponds with theoretical prediction already published for systems containing conducting polymers [37, 44, 57]. Here can be seen that higher content of PPy indicates stronger ER activity and thus higher yield stresses which are around 10 Pa for sample 2 and around 30 Pa for sample 3 at 3.0 kV/mm, respectively.

Further increase of PPy content in nanocomposite (sample 4) results in higher ER activity (Fig.33). Flow curves provide longer plateau of the shear stress which denotes that this suspension have a stronger chain-like structure under applied electric field.

Fig. 34 shows sample 5 with the highest content of PPy. At zero electric field strength suspension exhibits slight yield stress. With increasing electric field the higher yield stress is observed. Flow curves of this sample provide longer plateau than previous ones. Plateau is

getting longer with increasing electric field strength. Value of yield stress is around 125 Pa at E=3.0 kV/mm. It is necessary to say that this very strong ER effect was achieved by suspension containing only 5 wt. % of particles suspended in silicone oil.

Viscosity as a function of shear rate is shown in Figs. 35-39. Without an applied external electric field viscosity is nearly constant with increasing shear rate and thus exhibits Newtonian behavior for sample 1 and sample 2 (Fig. 35 and 36).

Other samples behave as non-Newtonian (viscosity decreases with increases shear rate). This is result of particles and oil interactions and pseudoplasticity increases with PPy content.

Under application of electric field viscosity increases significantly with electric field strength and decreases with increasing shear rate. At low shear rates viscosity exhibits the highest values because the electrostatic forces dominate in this region and thus the structure of chains between electrodes causes viscosity enhancement. At higher shear rates, viscosity decrease because the hydrodynamic forces become dominating over electrostatic ones. Suspensions show highly pseudoplastic character.

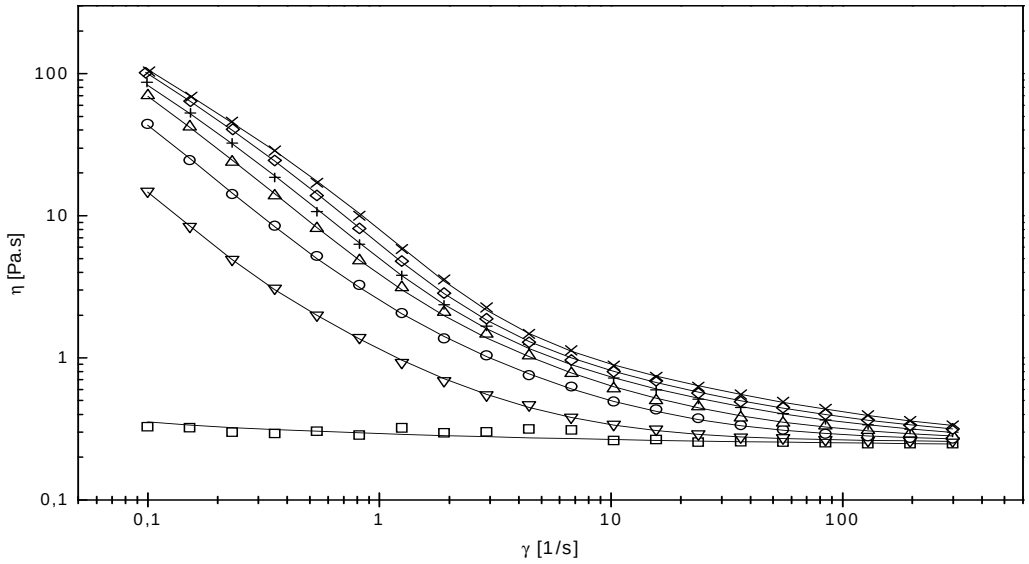

Fig. 35: Dependence of shear viscosity, η, on shear rate, γ, for sample 1 at various electric field strengths E (kV/mm): □ 0, ▽ 0.5, ○ 1.0, △ 1.5, + 2.0, ◇ 2.5, × 3.0. Solid lines represent Choi-Choi-Jhon model fit.

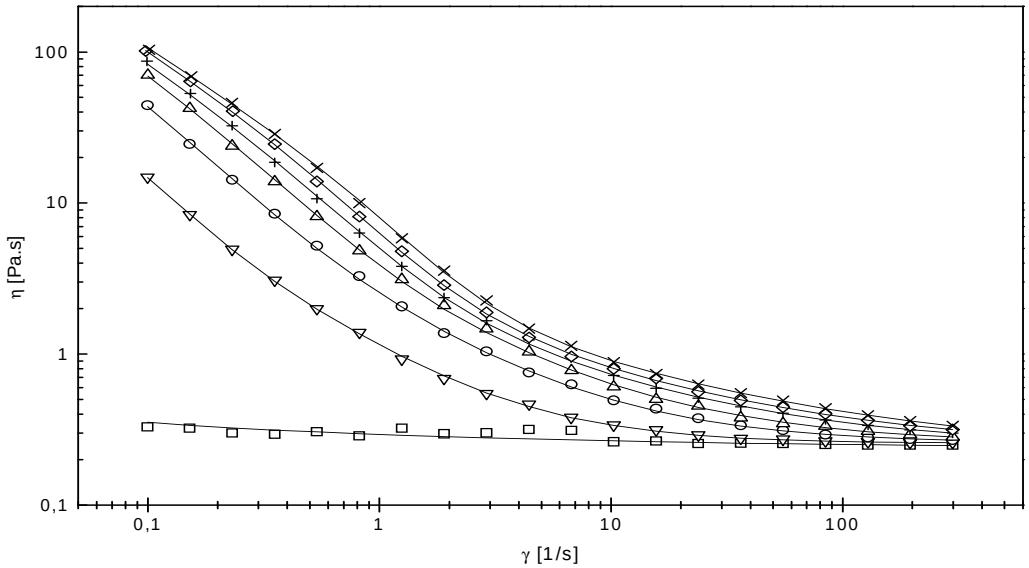

Fig. 36: Dependence of shear viscosity, η, on shear rate, γ, for sample 2 at various electric field strengths E (kV/mm): □ 0, ▽ 0.5, ○ 1.0, △ 1.5, + 2.0, ◇ 2.5, × 3.0. Solid lines represent Choi-Choi-Jhon model fit.

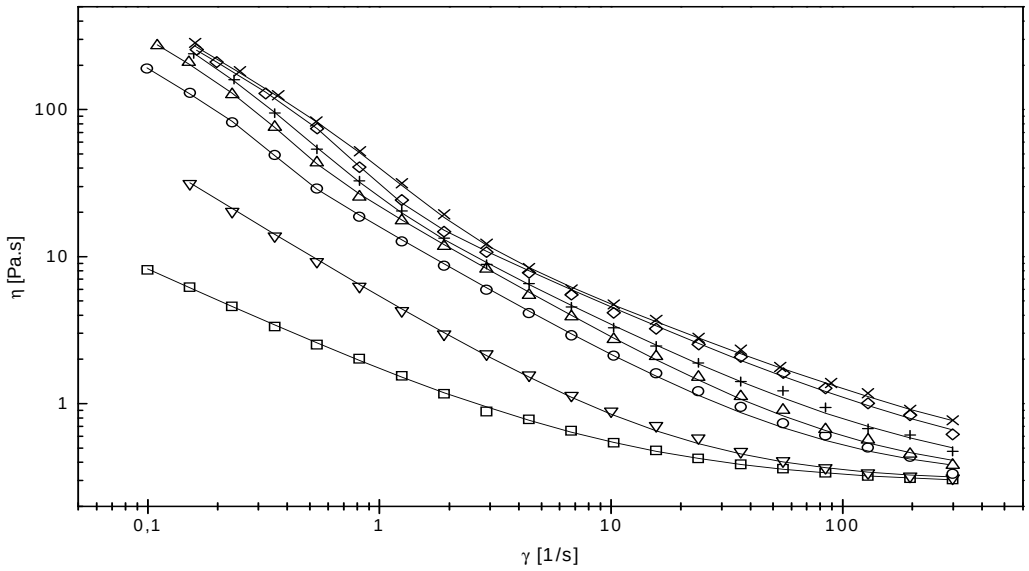

Fig. 37: Dependence of shear viscosity, η, on shear rate, γ, for sample 3 at various electric field strengths E (kV/mm): □ 0, ▽ 0.5, ○ 1.0, △ 1.5, + 2.0, ◇ 2.5, × 3.0. Solid lines represent Choi-Choi-Jhon model fit.

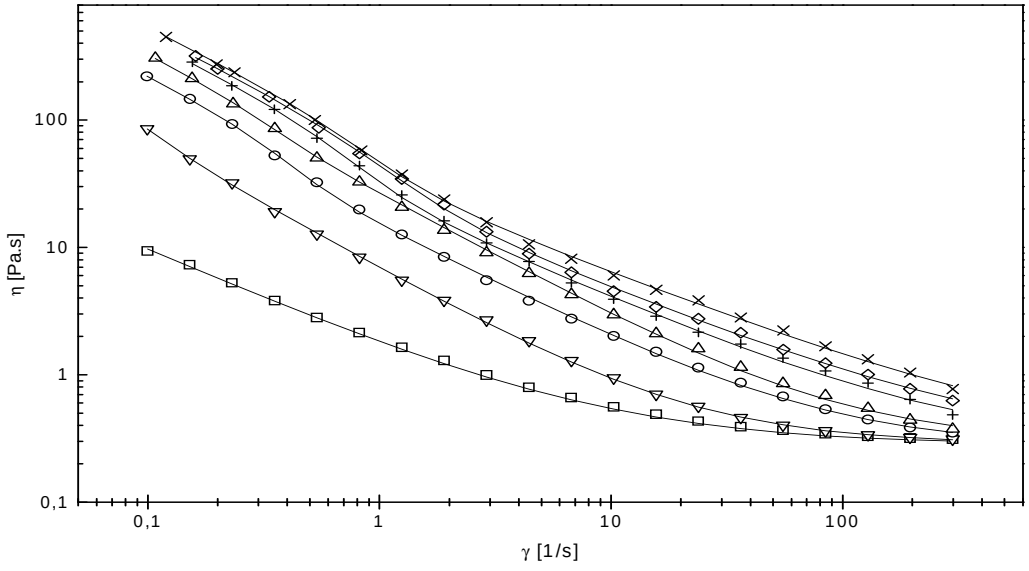

Fig. 38: Dependence of shear viscosity, η, on shear rate, γ, for sample 4 at various electric field strengths E (kV/mm): □ 0, ▽ 0.5, ○ 1.0, △ 1.5, + 2.0, ◇ 2.5, × 3.0. Solid lines represent Choi-Choi-Jhon model fit.

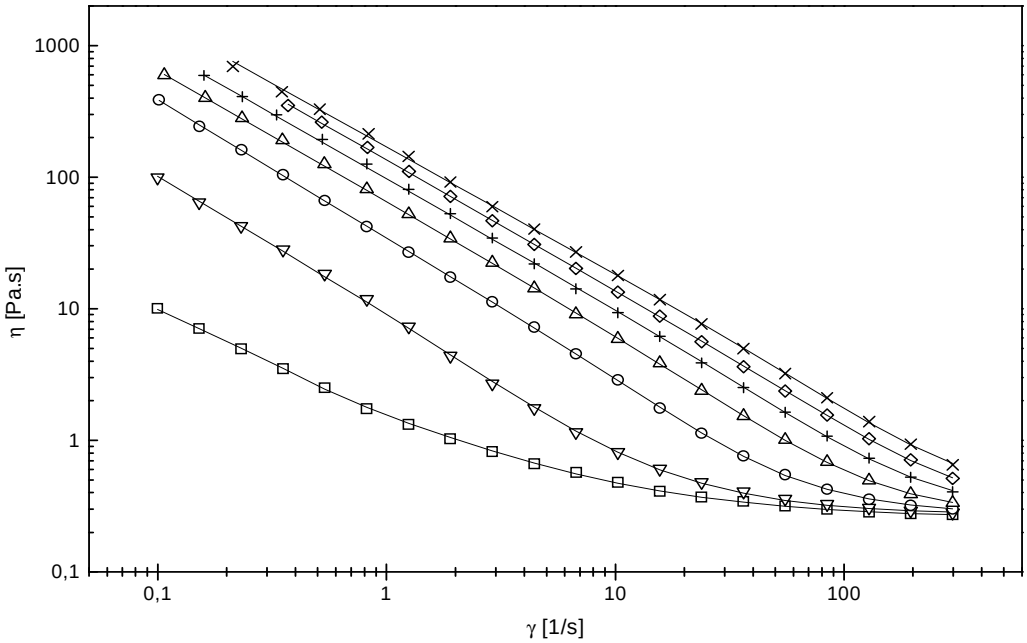

Fig. 39: Dependence of shear viscosity, η, on shear rate, γ, for sample 5 at various electric field strengths E (kV/mm): □ 0, ▽ 0.5, ○ 1.0, △ 1.5, + 2.0, ◇ 2.5, × 3.0. Solid lines represent Choi-Choi-Jhon model fit.

7.3 Current-voltage characteristics

Electric conductivity represents important parameter in design of ER suspensions because its large value causes electric losses and can bring electric break down of investigated systems. Figs. 40-44 show current as a function of time at various electric field strengths for samples 1-5. Measurement was performed just before ER experiments in the gap of rheometer without rotation.

Samples 1, 2 and 3 showed very low values of current passing throw suspensions in order of 10^{-6}-10^{-7} A which is close to resolution limit of electrometer used. Quite stable time dependence of current can be observed (Figs. 40, 41, 42).

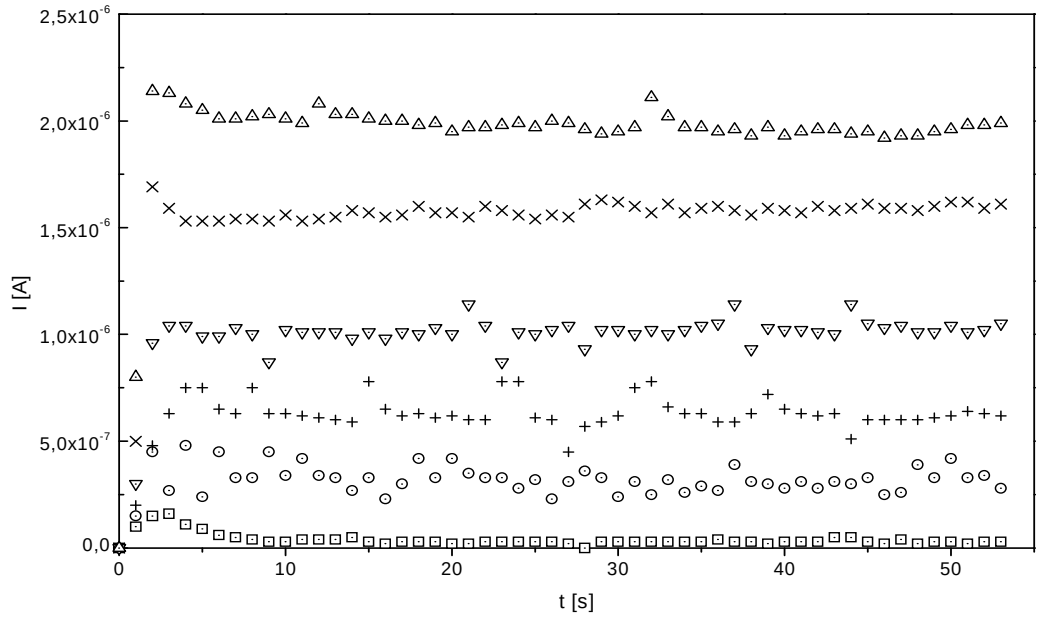

Fig. 40: Dependence of current, I, on time, t, for sample 1 at various electric field strengths E (kV/mm): □ 0.5, ○ 1.0, + 1.5, ▽ 2.0, × 2.5, △ 3.0.

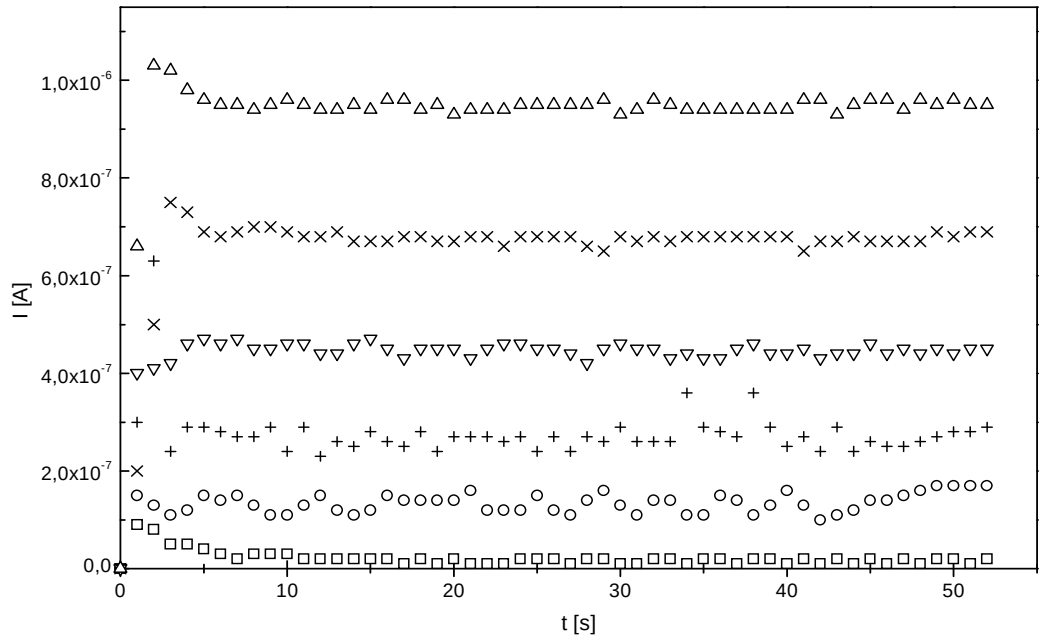

Fig. 41: Dependence of current, I, on time, t, for sample 2 at various electric field strengths E (kV/mm): □ 0.5, ○ 1.0, + 1.5, ▽ 2.0, × 2.5, △ 3.0.

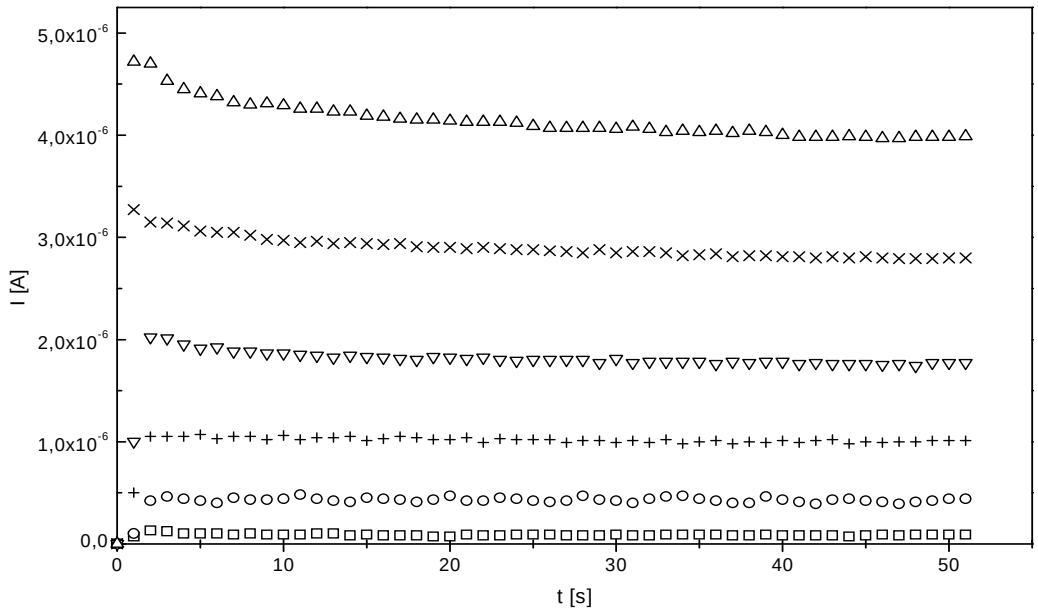

Fig. 42: Dependence of current I, on time, t, for sample 3 at various electric field strengths E (kV/mm): □ 0.5, ○ 1.0, + 1.5, ▽ 2.0, × 2.5, △ 3.0.

On the other hand samples 4 and 5 (Figs. 43 and 44) behaved in a different manner. Current continuously increases with time reaching equilibrium value at around 50 s as a consequence of electric field induced structure development.

Increasing amount of PPy caused increasing conductivity of suspensions, however in all samples its value was low enough to allow generate ER effect without electric breakdown in whole range of electric field strengths.

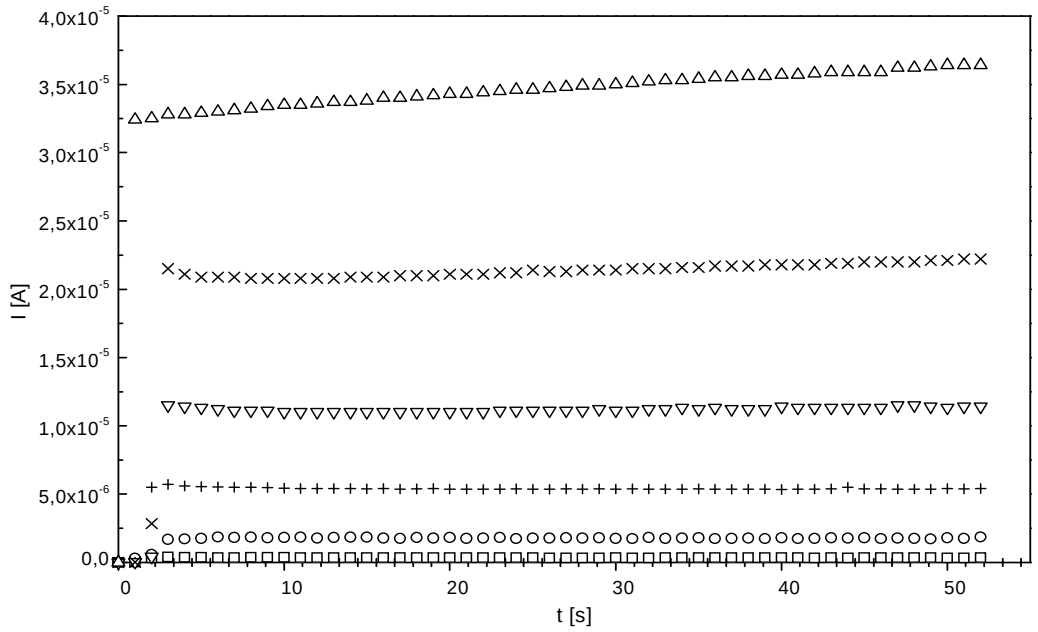

Fig. 43: Dependence of current, I, on time, t, for sample 4 at various electric field strengths E (kV/mm): □ 0.5, ○ 1.0, + 1.5, ▽ 2.0, × 2.5, △ 3.0.

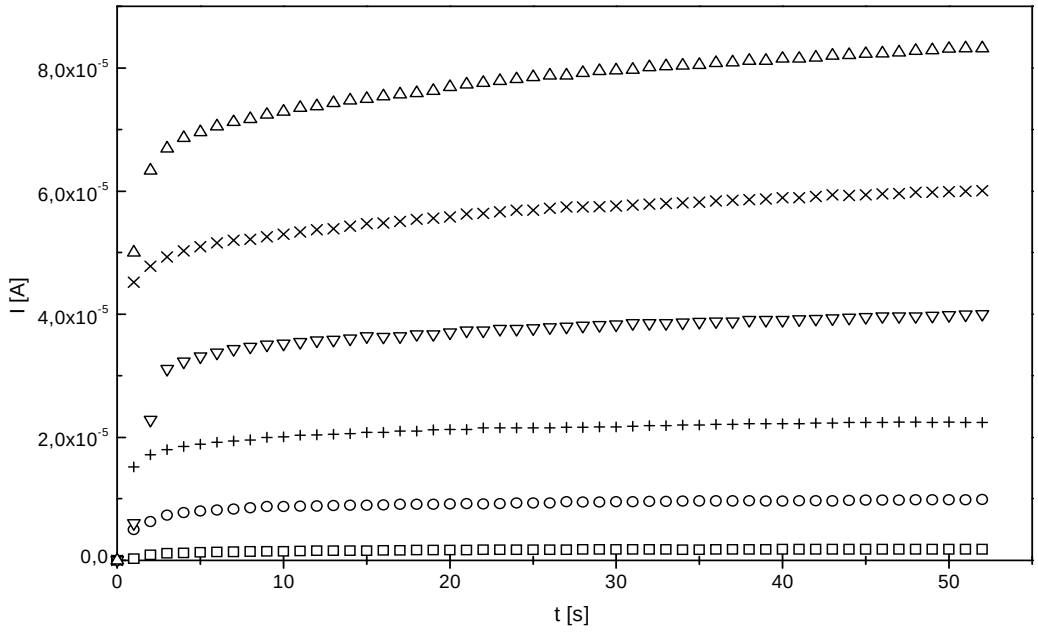

Fig. 44: Dependence of current, I, on time, t, for sample 5 at various electric field strengths E (kV/mm): □ 0.5, ○ 1.0, + 1.5, ▽ 2.0, × 2.5, △ 3.0.

Fig. 44 exhibits dependence of equilibrium current passing throw suspension as a function of used voltage. This dependency is nonlinear for all the samples providing non-ohmic character of suspensions conductivity. Sample 5 having highest content of PPy showed largest electrical conductivity.

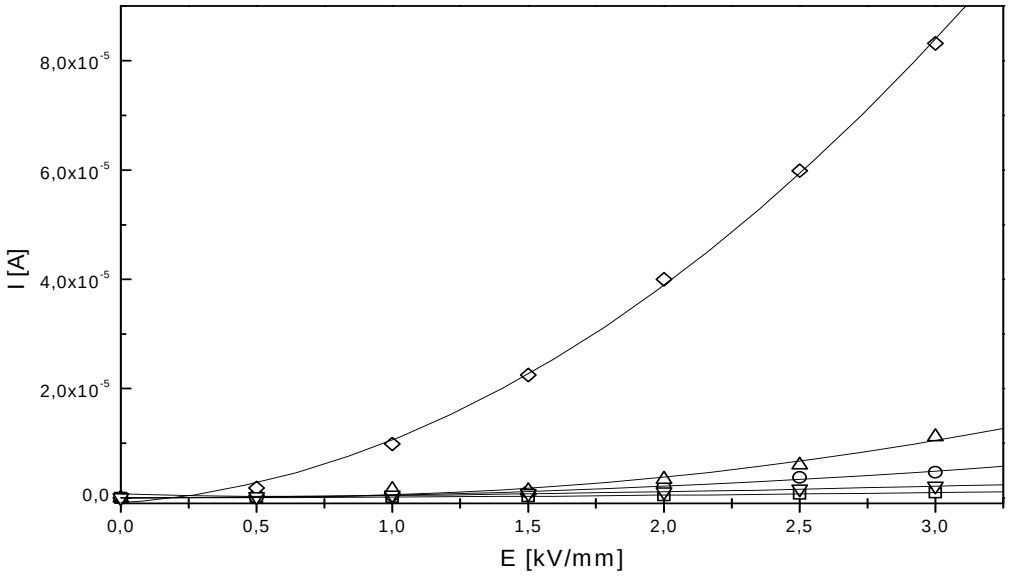

Fig. 45: Dependence of current, I, on electric field strength, E, where: □ sample 1, ▽ sample 2, ○ sample 3, △ sample 4, ◇ sample 5.

7.4 Dielectric properties

Dependence of dielectric properties such as dielectric constant, ε', and dielectric loss factor, ε'', on frequency are shown in Fig. 46. As can be seen dielectric constant, ε', decreases with frequency and this trend is more pronounced with increasing PPy content in nanocomposite particles forming dispersed phase of silicone oil suspensions. Dielectric loss factor, ε'', exhibits local maxima and their position is moved toward higher frequencies with increasing PPy content.

In order to describe dielectric spectra in Fig. 46 experimental data were fit using Havriliak-Negami model (eq. 11) [58] which can describe well behavior of investigated suspensions. Five parameters of this model were determined using least square method in Solver option of MS EXCEL and are shown in table 7.

$$\varepsilon^*_{HN}(\omega) = \varepsilon'_{\infty} + \frac{\Delta\varepsilon}{\left(1+(i\omega\cdot t_{rel})^a\right)^b} \qquad (11)$$

where ε'_{∞} is high frequency dielectric constant, ε_s' is static dielectric constant, $\Delta\varepsilon=(\varepsilon_s'-\varepsilon'_{\infty})$ is polarizability, ω is angular frequency (=2 π f), t_{rel} is the relaxation time, a and b are shape parameters which describe the symmetric and asymmetric broadening of the dielectric function, $0<a$, $a.b<1$. The parameters a and b are related to the limiting behavior of the dielectric function at low and high frequencies.

Table 7: Parameters of Havriliak-Negami model

	sample 1	sample 2	sample 3	sample 4	sample 5
ε'_{∞}	2.64	2.75	2.68	2.80	2.74
$\Delta\varepsilon$	0.76	0.81	1.39	1.49	1.77
t_{rel}	0.446	0.264	0.176	0.072	0.003
a	0.87	1.00	1.00	0.92	0.54
b	0.14	0.17	0.14	0.24	0.78
ε'_s	3.40	3.56	4.07	4.29	4.52

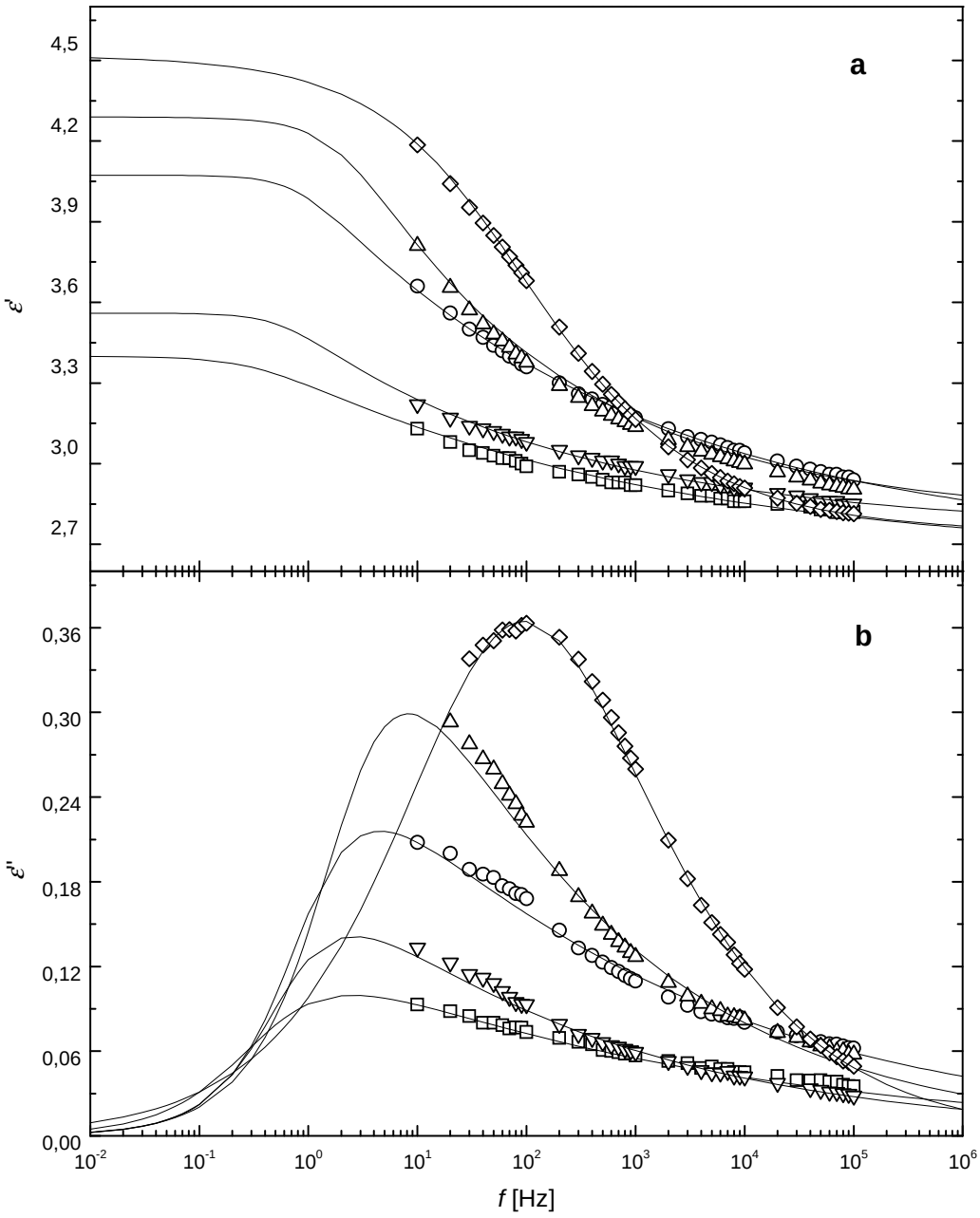

Fig. 46: Frequency spectra of dielectric constant (a), dielectric loss factor (b) where: □ sample 1, ▽ sample 2, ○ sample 3, △ sample 4, ◇ sample 5. Solid lines represent Havriliak-Negami model fit.

It is obvious from Fig. 46 and table 7 that polarizability, $\Delta\varepsilon$, as a measure of particle polarization, increases with content of PPy in the system. Dielectric loss factor, ε'', shows increasing values of maxima and peak position is shifted to higher frequencies, e.g. relaxation time, t_{rel}, of process decreases. Large polarizability, $\Delta\varepsilon$, optimal dielectric loss factor, ε'', and short relaxation time are parameters positively influencing intensity of ER effect. Correlation between electrorheological, dielectric and electric properties will be further discussed in chapter 8.

8 CORRELATION BETWEEN DIELECTRIC, ELECTRIC AND ELECTRORHEOLOGICAL PROPERTIES

Electrorheological behavior is result of complex adjustment of suspension properties. Among them suitable dielectric and electric properties seem to be crucial in design of electrorheological fluids.

Yield stress as the scale of electrorheological efficiency was chosen for correlation of electric, dielectric and electrorheological properties. For this purposes yield stress values obtained from Choi-Choi-Jhon model fit (tables 2–6) were used.

Dependence of yield stress on square of the electric field strength is shown in Fig.47. Yield stress at first increases rapidly while at higher electric field strengths it levels off. Values are significantly influenced with electrical conductivity of samples which increases with PPy content in nanocomposite particles (Fig.48). Yield stress of 126 Pa is obtained for most conducting sample 5 at highest electric field strength used (3 kV/mm).

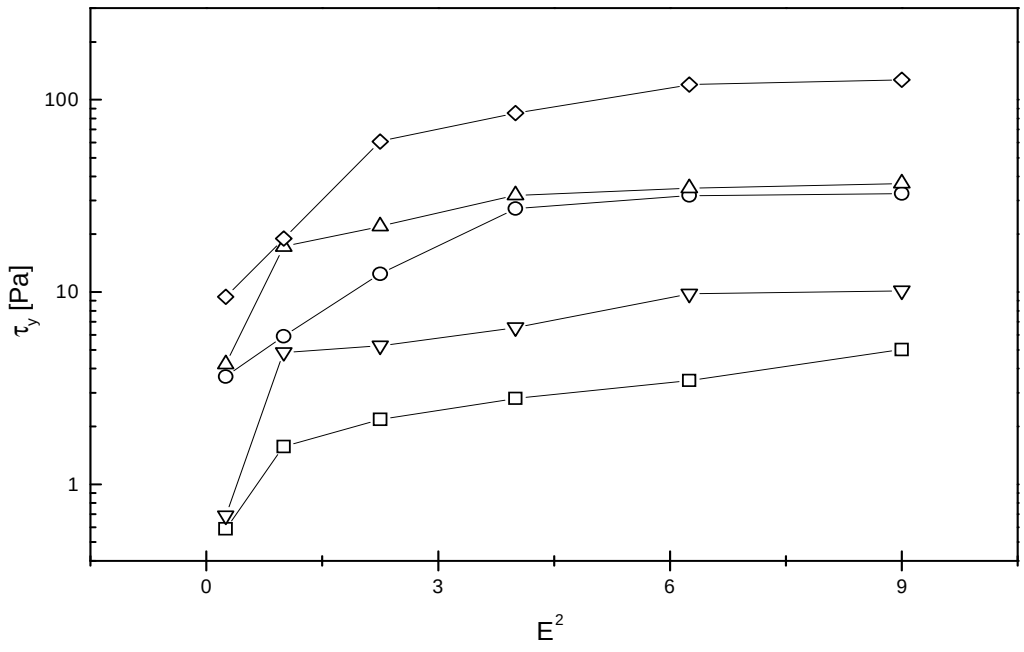

Fig. 47: Dependence of yield stress, $\tau_{y,}$ on square of the electric field strength, E^2, where: □ sample 1, ▽ sample 2, ○ sample 3, △ sample 4,◇ sample 5.

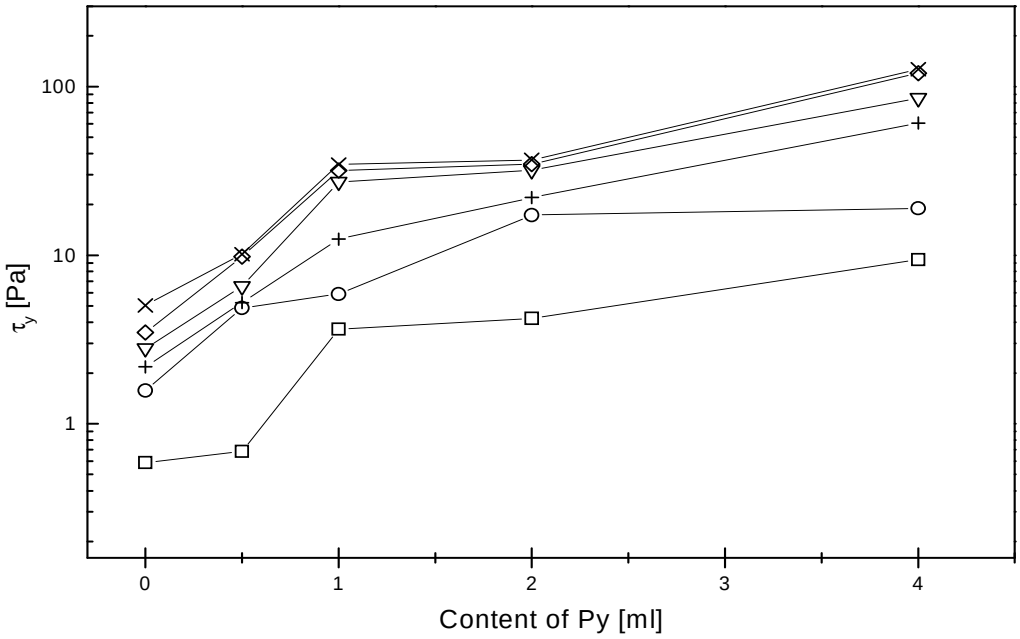

Fig. 48: Dependence of yield stress, τ_y, on content of pyrrole used during polymerization at various electric field strengths E (kV/mm): □ 0.5, ○ 1.0, + 1.5, ▽ 2.0, ◇ 2.5, × 3.0.

Furthermore, yield stress monotonically increases with polarizability as can be seen in Fig. 49. In order not to provide crowded curves data only for lowest (0.5 kV/mm) and highest (3.0 kV/mm) electric field strengths are presented. The others showed similar trends.

Fig.50 exhibits correlation between yield stress and relaxation time of the polarization process. Yield stress significantly decreases as the relaxation time decreases. It can be observed that above relaxation time value (ca 2.10^{-1} s) yield stress falls down rapidly. Appropriate polarizability followed with short relaxation time is necessary for generation of strong electrorheological effect.

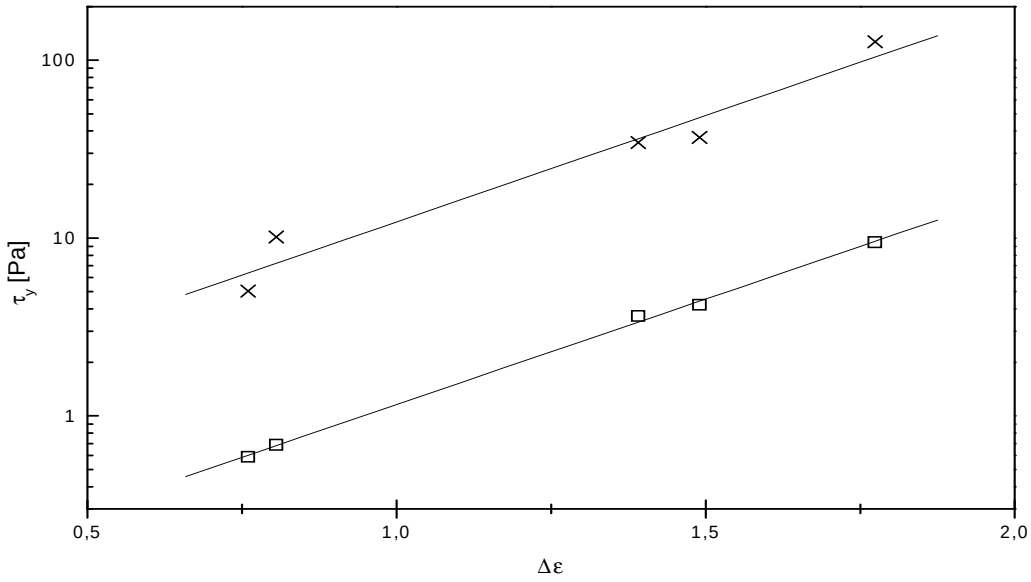

Fig. 49: Dependence of yield stress, $\tau_{y,}$ on polarizability, $\Delta\varepsilon$, at electric field strengths E (kV/mm): □ 0.5, × 3.0.

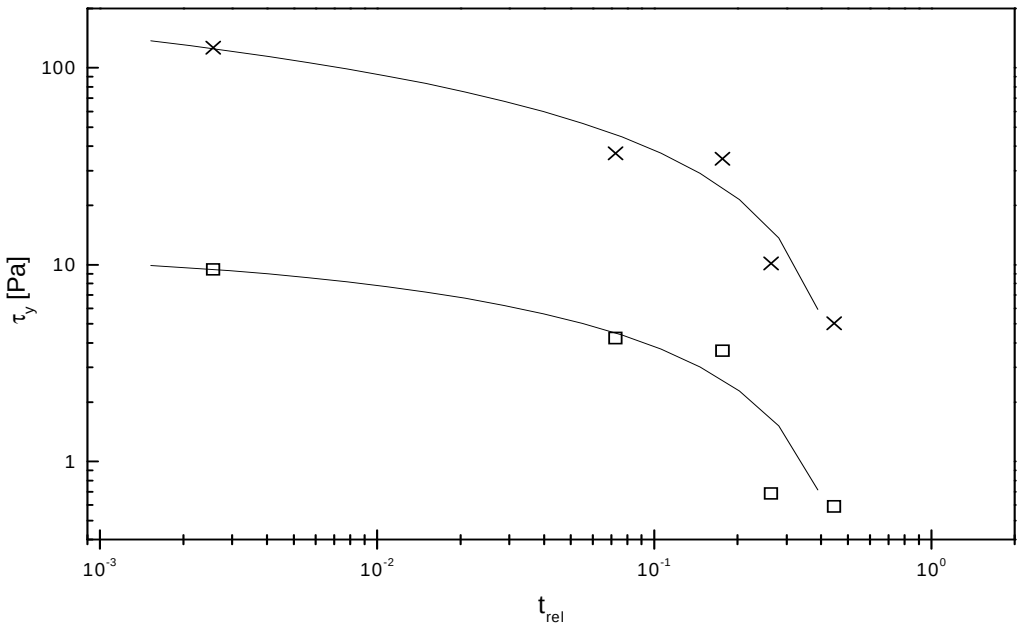

Fig. 50: Dependence of yield stress, $\tau_{y,}$ on relaxation time, t_{rel},, at electric field strengths E (kV/mm): □ 0.5, × 3.0.

CONCLUSION

Novel core-shell materials suitable for preparation of electrorheological suspensions have been developed. Titanate nanorods were synthesized as a core and shell layer consisted of various amount of polypyrrole. SEM analysis showed that rod like structure is preserved after polymerization of polypyrrole on surface of nanorods. Polypyrrole layer becomes more compact with increasing ratio of titanate nanorods and pyrrole used for polymerization.

Further, electrorheological, dielectric and electric properties of 5 wt. % silicone oil suspensions were determined. Titanate nanorods (sample 1) showed weakest electrorheological effect and its intensity increased with polypyrrole content in core-shell nanocomposites. Yield stress as a result of structural changes of suspensions upon application of electric field reached more than 120 Pa for suspension containing particles with highest content of polypyrrole (sample 5). Such an effect generated in only 5 wt. % suspension provides promising results for further applications.

Electrorheological behavior of suspensions strongly reflected electric and dielectric properties of materials used for their preparation. Increasing content of polypyrrole caused higher electrical conductivity of nanocomposites and changed dielectric properties in favorable manner. It was shown that enhanced polarizability of materials and reduced relaxation time (obtained from dielectric spectra) significantly rices intensity of electrorheological effect. Tayloring of core-shell materials seems to be promising way how to get very efficient electrorheological fluids suitable also for practical applications.

BIBLIOGRAPHY

[1] Winslow, W.M.: Methods and means of translating electrical impulses into mechanical force, US Patent 21 47 750, 1947

[2] Hao, T.: Electrorheological Fluids: The non-aqueous suspensions, 1st ed., Cambridge, Massachusetts, 2005, ISBN-13: 978-0-4444-52180

[3] Espin, M.J.; Delgado, A.V.; Gonzales-Caballero, F.; Rejon, L.: Rheological properties of a model colloidal suspension under large electric fields of different waveforms, Journal of Non-newtonian Fluid Mechanics, 146, 2007, 125-135

[4] Espin, M.J.; Plocharski, J.: Effect of pollution on the interfacial properties of electrorheological suspensions, Colloids and Surfaces A-Physicochemical and Engineering Aspects, 306, 2007, 126-136

[5] Sung, B.H.; Choi, U.S.; Jang, H.G.; Park, Y.S.: Novel approach to enhance the dispersion stability of ER fluids based on hollow polyaniline sphere particles, Colloids and Surfaces A-Physicochemical and Engineering Aspects, 274, 2006, 37–42

[6] Akhavan, J.: Electro-rheological polymers, Proceedings of the institution of mechanical engineers part G-Journal of Aerospace Engineering, 221, 2007, 577-587

[7] Winslow, W.M.: Induced fibration of suspensions, Journal of Applied Physics, 20, 1949, 1137-1140

[8] Shen, M.; Cao, J.G.; Zhu, J.T.; Xue, H.T.; Zhow, L.W.: Van der Waals interaction in colloidal giant electrorheological systems, International Journal of Modern Physics B, 19, 2005, 1170-1176

[9] Misono, Y.; Negita, K.: Shear-induced particle rotation and its effect on electrorheological properties and dielectric properties in cellulose suspension, Physical Review E, 70, 2004, 061412

[10] Wen, W.J.; Huang, X.X.; Yang, S.H.; Lu, K.Q.; Sheng, P.: The giant electrorheological effect in suspensions of nanoparticles, Nature Materials, 11, 2003, 727-730

[11] Wang, BX.; Zhao, XP.; Zhao, Y.; Ding, CL.: Titanium oxide nanoparticles modified with chromium ion and its giant electrorheological activity, Composites Science and Technology, 67, 2007, 3031-3038

[12] Huang, X.; Wen, W.; Yang S.; Sheng P.: Mechanisms of the giant electrorheological effect, Solid State Communications, 139, 2006, 581–588

[13] Boissy, C.; Atten, P.; Foule, J.N.: On a negative electrorheological effect, Journal of Electrostatics, 35, 1995, 13-20

[14] Koyama, K.; Minagawa K.; Watanabe, T.; Kumakura, Y.; Takimoto, J.: Electromagneto-rheological effects in paralel-field and crossed-field systems, Journal of Non-newtonian Fluid Mechanics, 58, 1995, 195-206

[15] Komoda, Y.; Sakai, N.; Rao, T.N.; Tryk, D.A.; Fujishima, A.: Photoelectrorheological phenomena involving TiO_2 particle suspensions, Langmuir 14, 1998, 1081-1091

[16] Parthasarathy, M.; Klingenberg, D.J.: Electrorheology: Mechanisms and models, Materials Scince & Engineering R-Reports, 17, 1996, 57-103

[17] Schwarz M.: Encyclopedia of smart material, Volume 1, John Wiley & Sons, 2002, 376-390, ISBN 978-0-471-17780-7

[18] Cho, M.S.; Choi, H. J.; Jhon, M.S.: Shear stress analysis of a semiconducting polymer based electrorheological fluid system, Polymer, 46, 2005, 11484-11488

[19] Jianbo, Y.; Xiaopeng, Z.: Electrorheological properties of titanate nanotubes suspensions, Colloids and Surfaces A-Physicochemical and Engineering Aspects, 329, 2008, 153-160

[20] Chen, L.F.; Ong, C.K.; Neo, C.P.; Varadan, V.V.; Varadan, V.K.:Microwave electronics - measurement and materials characterization, John Wiley & Sons, 2004, ISBN 978-0-470-84492-2

[21] Wei C., Zhu Y., Jin Y., Yang X., Li C.: Fabrication and characterization of mesoporous TiO_2 /polypyrrole-based nanocomposite for electrorheological fluid, Materials Reasearch Bulletin, 43, 2008, 3263-3269

[22] Hou, J.; Shi, L.; Zhu, Q.: Electrorheological properties and structure of ($BaTiO(C_2O_4)NH_2CONH_2$), Journal of Solid State Chemistry, 179, 2008, 1874-1878

[23] Kanu, R.; Shaw, M.: Enhanced electrorheological fluids using anisotropic particles, Journal of Rheology, 42, 1998, 657-670

[24] Gong, X.Q.; Wu, J.B.; Huang, X.X.; Wen, W.J.; Sheng, P.: Influence of liquid phase on nanoparticle-based giant electrorheological fluid, Nanotechnology, 19, 2008, 165602

[25] Jordan, M.; Schwendt, A.; Hill, D.; Burton, S.; Makris, N.: Zeolite-based electrorheological fluids: Testing, modeling and instrumental artifacts, Journal of Rheology, 41, 1997, 75-91

[26] Katsikopoulos, P; Zukoski, C.F.: Effects of electrode morphology on the electrorheological response, In proceedings of the 4th. international conference of electrorheological fluids, Singapore, 1994, 256-263

[27] Hong, C.H.; Choi, H.J.: Shear stress analysis of phosphorylated potato starch based electrorheological fluid, Korea-Australia Rheology Journal, 19, 2007, 221-225

[28] Negita, K.; Itou, H.; Yakou, T.: Electrorheological effect in suspension composed of strach powder and silicone oil, Journal of Colloid and Interface Science, 209, 1999, 251-254

[29] Huo, L.; Liao, F.H.; Li, R.J; Zhang, S.H.; Zhang, O.; Ma, S.Z.; Xu, M.Y.; Lu, Y.m.: Electrorheological properties of chitosan nitrate suspension, Colloids and Surface A-Physicochemical and Engineering Aspects, 316, 2008, 125-130

[30] Yoon, D.J.; Kim, Y.D.: Electrorheological properties of polypyrrole-SnO_2 – methylcellulose nanocomposite suspensions, Journal of Material Science, 42, 2007, 5534-5538

[31] Song, D.H.; Lee, H.M.; Lee, K.H.; Choi, H.J.: Intercalated conducting polyaniline-clay nanocomposites and their electrical characteristics, Journal of Physics and Chemistry of Solids, 69, 2008, 1383-1385

[32] Sung, J.H.; Lee, I.; Choi, J.H.: Electrorheological respons of polyaniline-TiO_2 composite suspensions, International Journal of Modern Physics B, 19, 2005, 1128-1134

[33] Sung, B.H.; Ko, Y.G.; Choi, U.S.: Novel synthesis and electrorheological properties of monodispersed submicrone-sized hollow polyaniline dicarboxylate salt form suspensions, Colloids and Surfaces A-Physicochemical and Engineering Aspects, 292, 2007, 217-223

[34] Kim, D.H.; Kim, Y.D.: Electrorheological properties of polypyrrole and its composite ER fluids, Journal of Industrial and Engineering Chemistry, 13, 2007, 879-894

[35] Kim, Y.D.; Song, I.C.: Electrorheological and dielectric properties of polypyrrole dispersions, Journal of Material Science, 37, 2002, 5051-5055

[36] Zheng, L.; Deng, Z.X.; Li, Y.N.: Electrorheological properties of titania particle with CE a Y composite doping as an anhydrous ER fluids, In proceedings of the 9th international conference on electorheological (ER) fluids and magnetorheological (MR) suspensions, China, 2005, 121-126

[37] Lim, J.Y.; Kim, S.T.; Park, B.J.; Choi, H.J.: Preparation and electrorheological characteristics of PANI/MWNT nanocomposite, International Journal of Modern Physics B, 21, 2007, 5003-5009

[38] Kim, Y.D.; Kim, J.H.: Synthesis of polypyrrole-SBS composites and particle size efect on the electrorheological properties of their suspensions, Synthetic Metals, 158, 2008, 479-483

[39] Zhang, K.; Lim, J.Y.; Choi, H.J.: Core-shell structured carbon nanotube/ poly(methyl methacrylate) composite and its electrorheological activity, Diamond and Related Materials, 17, 2008, 1604-1608

[40] Kawai, A.; Ide, Y.; Inoue, A.; Ikzaki, F.: Electrorheology of miscele blended liquid cristalline polymer: A dielectric property approach, Journal of Chemical Physics, 109, 1998, 4587-4591

[41] Gercek, B.;Yavuz, M.; Yilmaz, H.; Sari, B.; Unal, H.I.: Comparison of electrorheological of some polyaniline derivatives, Colloids and Surfaces A-Physicochemical and Engineering Aspects, 299, 2007, 124–132

[42] Negita, K.; Misono, Y.; Yamaguchi, T.; Shinagawa, J.: Dielectric and electrical properties of electrorheological carbon suspensions, Journal of Colloid and Interface Science, 321, 2008, 452-458

[43] Yin, J.; Zhao, X.P.; Xia, X.; Xiang, L.; Qiao, Y.P.: Electrorheological fluids based on nano-fibrous polyaniline, Polymer, 49, 2008, 4413–4419

[44] Kim, S.G.; Lim, Y.J.; Sung, J.H.; Choi, J.H.; Seo, Y.: Emulsion polymerized polyaniline synthesized with dodecylbenzene-sulfonic acid and its electrorheological characteristics: Temperature effect, Polymer, 48, 2007, 6622-6631

[45] Wang, B.X.; Zhao, Y.; Zhao, X.P.: The wettability, size effect and electrorheological activity of modified titanium oxide nanoparticles, Colloids and Surface A-Physicochemical and Engineering Aspects, 295, 2007, 27-33

[46] Mezzasalma, S.A.; Koper, G.J.M.: Semiclassical approach to electrorheological fluids: Influence of solid volume fraction on the suspension yield stress, Colloid and Polymer Science, 280, 2002, 160-166

[47] Hanaoka, R.; Murakumo, M.; Anzai, H.; Sakurai, K.: Effects of electrode surface morphology on electrical response of electrorheological fluids, IEEE Transactions on Dielectrics and Electrical Insulation, 9, 2002, 10-16

[48] Tsuda, K.; Hirose,Y.; Ogura, H.; Otsubo, Y.: Effect of electric fields on the surface profiles of electrorheological suspensions, Colloids and Surface A-Physicochemical and Engineering Aspects, 324, 2008, 228-233

[49] Abu-Jdayil, B.; Brunn, P.O.: Effects of coating on the behavior of electrorheological fluids in torsional flow, Smart Materials & Structures, 6, 1997,509–520

[50] Choi, S.B.; Thompson, B.S.; Gandhi, M.V.: An experimental investigation on smart laminated composite structures featuring embedded electrorheological fluid domains for vibration-control applications, Composites Engineering, 2, 1992, 543–559.

[51] Abu-Jdayil, B.; Asoud, H.; Brunn, P.O.: Effect of polymer coating on the behaviour of an electrorheological fluid, Materials and Design, 28, 2007, 928-940

[52] Foulc, N.J.; Atten P.; Felici N.: Conductive model of particle interaction in an electrorheological fluids, Comptes rendus de l academie des science serie II, 317 1993, 5-11

[53] Rankin, P.J.; Klingenberg, D.J.: The electrorheology of barium titanate suspensions, Journal of Rheology, 42, 1998, 639-656

[54] Choi, S.B.; Han, S.S.: H_∞ control of electrorheological suspension system subjected to parameters uncertainties, Mechatronics, 12, 2003, 639-657

[55] Chandrasekhar, P.: Conducting polymers, fundamentals and applications: a practical approach, Norwell, Massachusetts, 1999, 381-384, ISBN 0-7923-8564-0

[56] Cheng, Q., He, Y., Pavlinek, V., Li, Ch., Saha, P.: Surfactant-assisted polypyrrole/titanate composite nanofibers: Morphology, structure an electrical properties, Synthetic Metals, 158, 2008, 953-958

[57] Fang, F:F.; Kim, H.J; Choi, H.J; Seo,Y.: Organic/inorgani hybrid of polyaniline/BaTiO3 and their electrorheological and dielectric characteristics, Journal of Applied Polymer Science, 105, 2007, 1853-1860

[58] Kremer, F.; Schonhals, A.: Broadband dielectric spectroscopy, Berlin, Germany, 2003, 10-65, ISBN 3-540-43407-0

LIST OF ABBREVIATIONS

ER	electrorheological
$\dot{\gamma}$	shear rate
E	electric field strength
H	magnetic field strength
MR	magnetorheological
τ	shear stress
η	shear viscosity
η_p	plastic viscosity
τ_y	yield stress
PNQR	poly(napthalene quinone)radical
ε	dielectric constant
C_0	capacitance of empty condenser filled with air
C	capacitance of condenser with dielectric between electrodes
ε^*	complex dielectric constant
ε'	dielectric constant
ε''	dielectric loss factor
tan δ	dielectric loss tangent
ω, f	angular frequency, frequency
$\Delta\varepsilon$	polarizability
ε'_s	static dielectric constatnt
ε'_∞	high frequency dielectric constant
TiO_2	titanium dioxide
$BaTiO_3$	Barium titanate
PANI	polyaniline

PPy	polypyrrole
MWCNT	multi-wall carbon nanotubes
E_c	critical electric field strength
c	particle concentration
g	constant explained particle geometry
ρ	particle density
$\bar{\nu}$	average volume
T	temperature
k_B	Boltzmans' constant
ε_m	dielectric constant of continuous phase
ε_p	dielectric constant of particles
E^2	square of electric field strength
$\Delta\tau$	field induced change in shear stress
DBSA	dodecyl-benzen sulfonic acid
PETG	polyethylene glycol tereptahalate
TNt	titanate
NaOH	sodium hydroxide
SEM	scanning electron microscopy
CTAB	cetyltrimethylammoniumbormid
η_c	specific viscosity
σ_c	specific conductivity
α,	coefficient related to decreasing in the shear stress
t_1, t_2	time constants
η_∞	shear viscosity in high shear rate in the absence of the electric field
β	exponent falls to interval <0;1>

a, b	shape parameters
I	current
t	time

LIST OF FIGURES

Fig. 1: Schematic diagram of ER suspension (a) without applied external electric field, (b) with applied external electric field, (c) with applied shear flow and external electric field. [6] 12

Fig. 2: Schematic diagram of creating columns under applied electric field [11]. 13

Fig. 3: *Phase separation under an electric field due to electrophoresis, which leads to the negative ER effect [2].* 14

Fig. 4: Schematic illustration of particle organization in EMR effect. H represents applied magnetic field and E represents electric field [2]. 14

Fig. 5: *Dependence between shear stress and shear rate for poly (napthalene quinone) radical (PNQR) in silicone oil at various electric field strengths [18].* 17

Fig. 6: *Dependence between shear viscosity and shear rate for poly (naphthalene quinone) radical (PNQR) in silicone oil under four various electric field strengths [18].* 18

Fig. 7: *Schematic illustration of a dielectric between two electrodes [20].* 19

Fig. 8: *Dielectric spectra of electrorheological materials (Na-titanate nanotube (circle points) and H-titanate nanotube (square points)) [19].* 20

Fig. 9: *Molecular structure of polyaniline [2]* 23

Fig. 10: *Dependence between yield stress and electric field strength. [33]* 24

Fig. 11: *Molecular structure of polypyrrole [2]* 24

Fig. 12: *Dependence between yield stress and electric field strength at various content of polypyrrole [36].* 25

Fig. 13: *Dependence of static yield stress against intensity of electric field of* $BaTiO((C_2O_4)NH_2CONH_2)$ *particles in silicone oil (a) sample with least shell content, (b) sample with medium shell content, (c) sample with higher shell content [22].* 26

Fig. 14: Dependence between electric field strength and electric field viscosity of various polyaniline derivates [41]. 29

Fig. 15: Dependence between shear stress and external electric field of various polyaniline derivates [41]. 30

Fig. 16: *Shear stress vs. frequency of the electric field (1 kV/mm) at various shear rates [42].* 31

Fig. 17: Dependence between shear stress and shear rate of DBSA-doped PANI based ER suspension at various temperatures [44]. 32

Fig. 18: Dependence of yield stress against volume fraction of PPy-SnO_2-methylcelulose nanocomposite suspension at various electric field strengths [30]. 32

Fig. 19: Illustration of three operating modes in ER dampers [53]. 34

Fig. 20: Illustration of two clutches includes two plates or rotors [53]. 35

Fig. 21: The ER valve with electrodes on the both sides of the tube trough which ER active suspension flows [53]. 36

Fig. 22: Steel autoclave for preparation of TNt nanorods 39

Fig. 23 : Apparatus for preparation of core-shell composites (1 - mixing device, 2 – flask with dropper, 3 – three-necks flask, 4 – cooling medium, 5 – thermometer, 6 – pot)..... 40

Fig. 24: Schematic formation mechanism for the PPy/TNt composite[56]..... 41

Fig. 25: SEM image of sample 1..... 44

Fig. 26: SEM image of sample 2..... 45

Fig. 27: SEM image of sample 3..... 45

Fig. 28: SEM image of sample 4..... 46

Fig. 29: SEM image of sample 5..... 46

Fig. 30: Dependence of shear stress, τ, on shear rate, γ, for sample 1 at various electric field strengths E (kV/mm): □ 0, ○ 0.5 , ◇ 1.0, △ 1.5, ▽ 2.0, + 2.5, × 3.0. Solid lines represent Choi-Choi-Jhon model fit. 47

Fig. 31: Dependence of shear stress, τ ,on shear rate, γ, for sample 2 at various electric field strengths E (kV/mm): □ 0, ○ 0.5 , ◇ 1.0, △ 1.5, ▽ 2.0, + 2.5, × 3.0. Solid lines represent Choi-Choi-Jhon model fit. 48

Fig. 32: Dependence of shear stress, τ ,on shear rate, γ, for sample 3 at various electric field strengths E (kV/mm): □ 0, ○ 0.5 , ◇ 1.0, △ 1.5, ▽ 2.0, + 2.5, × 3.0. Solid lines represent Choi-Choi-Jhon model fit. 48

Fig. 33: Dependence of shear stress, τ ,on shear rate, γ, for sample 4 at various electric field strengths E (kV/mm): □ 0, ○ 0.5 , ◇ 1.0, △ 1.5, ▽ 2.0, + 2.5, × 3.0. Solid lines represent Choi-Choi-Jhon model fit. 49

Fig. 34: Dependence of shear stress, τ ,on shear rate, γ, for sample 5 at various electric field strengths E (kV/mm): □ 0, ○ 0.5 , ◇ 1.0, △ 1.5, ▽ 2.0, + 2.5, × 3.0. Solid lines represent Choi-Choi-Jhon model fit. 49

Fig. 35: Dependence of shear viscosity, η, on shear rate, γ, for sample 1 at various electric field strengths E (kV/mm): □ 0, ▽ 0.5, ○ 1.0, △ 1.5, + 2.0, ◇ 2.5, × 3.0. Solid lines represent Choi-Choi-Jhon model fit. 54

Fig. 36: Dependence of shear viscosity, η, on shear rate, γ, for sample 2 at various electric field strengths E (kV/mm): □ 0, ▽ 0.5, ○ 1.0, △ 1.5, + 2.0, ◇ 2.5, × 3.0. Solid lines represent Choi-Choi-Jhon model fit. 54

Fig. 37: Dependence of shear viscosity, η, on shear rate, γ, for sample 3 at various electric field strengths E (kV/mm): □ 0, ▽ 0.5, ○ 1.0, △ 1.5, + 2.0, ◇ 2.5, × 3.0. Solid lines represent Choi-Choi-Jhon model fit. 55

Fig. 38: Dependence of shear viscosity, η, on shear rate, γ, for sample 4 at various electric field strengths E (kV/mm): □ 0, ▽ 0.5, ○ 1.0, △ 1.5, + 2.0, ◇ 2.5, × 3.0. Solid lines represent Choi-Choi-Jhon model fit. 55

Fig. 39: Dependence of shear viscosity, η, on shear rate, γ, for sample 5 at various electric field strengths E (kV/mm): □ 0, ▽ 0.5, ○ 1.0, △ 1.5, + 2.0, ◇ 2.5, × 3.0. Solid lines represent Choi-Choi-Jhon model fit. 56

Fig. 40: Dependence of current, I, on time, t, for sample 1 at various electric field strengths E (kV/mm): □ 0.5, ○ 1.0, + 1.5, ▽ 2.0, × 2.5, △ 3.0. 58

Fig. 41: Dependence of current, I, on time, t, for sample 2 at various electric field strengths E (kV/mm): □ 0.5, ○ 1.0, + 1.5, ▽ 2.0, × 2.5, △ 3.0. 58

Fig. 42: Dependence of current I, on time, t, for sample 3 at various electric field strengths E (kV/mm): □ 0.5, ○ 1.0, + 1.5, ▽ 2.0, × 2.5, △ 3.0. 59

Fig. 43: Dependence of current, I, on time, t, for sample 4 at various electric field strengths E (kV/mm): □ 0.5, ○ 1.0, + 1.5, ▽ 2.0, × 2.5, △ 3.0. 60

Fig. 44: Dependence of current, I, on time, t, for sample 5 at various electric field strengths E (kV/mm): □ 0.5, ○ 1.0, + 1.5, ▽ 2.0, × 2.5, △ 3.0. 60

Fig. 45: Dependence of current, I, on electric field strength, E, where: □ sample 1, ▽ sample 2, ○ sample 3, △ sample 4, ◇ sample 5. 61

Fig. 46: Frequency spectra of dielectric constant (a), dielectric loss factor (b) where: ☐ sample 1, ▽ sample 2, ○ sample 3, △ sample 4, ◇ sample 5. Solid lines represent Havriliak-Negami model fit. 63

Fig. 47: Dependence of yield stress, $\tau_{y,}$ on square of the electric field strength, E^2, where: ☐ sample 1, ▽ sample 2, ○ sample 3, △ sample 4,◇ sample 5. 65

Fig. 48: Dependence of yield stress, $\tau_{y,}$ on content of pyrrole used during polymerization at various electric field strengths E (kV/mm): ☐ 0.5, ○ 1.0, ＋ 1.5, ▽ 2.0, ◇ 2.5, × 3.0...... 66

Fig. 49: Dependence of yield stress, $\tau_{y,}$ on polarizability, $\Delta\varepsilon$, at electric field strengths E (kV/mm): ☐ 0.5, × 3.0...... 67

Fig. 50: Dependence of yield stress, $\tau_{y,}$ on relaxation time, t_{rel},, at electric field strengths E (kV/mm): ☐ 0.5, × 3.0...... 67

LIST OF TABLES

Table 1: Composition of samples..... 41
Table 2: Parameters of the Choi-Choi-Jhon model for sample 1..... 50
Table 3: Parameters of the Choi-Choi-Jhon model for sample 2..... 51
Table 4: Parameters of the Choi-Choi-Jhon model for sample 3..... 51
Table 5: Parameters of the Choi-Choi-Jhon model for sample 4..... 51
Table 6: Parameters of the Choi-Choi-Jhon model for sample 5..... 52
Table 7: Parameters of Havriliak-Negami model 62